UNIVERSITY OF CALIFORNIA, SAN DIEGO

Mechanisms of Slowed Conduction During Ventricular Volume Loading

A dissertation submitted in partial satisfaction of the
requirements for the degree Doctor of Philosophy
in Bioengineering

by

Robert W. Mills

Committee in charge:

Professor Andrew D. McCulloch, Chair
Professor Wayne Giles
Professor Wilbur Lew
Professor Sanjiv Narayan
Professor Jeffrey Omens

2006

The dissertation of Robert W. Mills is approved, and it is acceptable in quality and form for publication on microfilm:

_____

_____

_____

_____

_____

Chair

University of California, San Diego

2006

TABLE OF CONTENTS

LIST OF FIGURES

LIST OF TABLES

ACKNOWLEDGEMENTS

This dissertation represents a portion of five years of research conducted within the Cardiac Mechanics Research Group in the Department of Bioengineering at the University of California, San Diego.

I would like to thank Dr. Andrew McCulloch for his academic and financial support; I could always count on him for multiple insights into attacking the various obstacles that arose and for improving my presentations and publications. I would also like to thank my thesis committee for their input and assistance along the way, especially: Dr. Wayne Giles for helping me with electrophysiology on a cellular\channel basis, Drs. Wilbur Lew and Sanjiv Narayan for improving my clinical knowledge and generally broadening my cardiology jargon, and Dr. Jeffrey Omens for helping me upgrade and keep my experimental equipment in working order.

Although he might not recognize these things anymore, I would like to thank Derrick Sung for the basis he provided in terms of the experimental setup and analysis code. I would like to thank Richard Pavelec for teaching me the necessary surgical techniques, Zhuangjie Li for his assistance in my early studies, and Biguang Yao for his assistance and especially for watching my back during studies, as trying to keep everything running and take data at the same time nearly drove me mad, and he attended to details while I was preoccupied. I would also like to thank Hunaid Gurji and Adam Wright, who as part of learning techniques from me, similarly helped keep things running and acted as beta-testers for my analysis code.

I also must acknowledge the assistance I received from the Cardiac Mechanics Research Group, as everyone past and present helped in little ways: giving me quick technical suggestions or advice on navigating campus bureaucracy, or simply adding some levity to my day. I would especially like to thank Sarah Healy

and Jeff Saucerman for talking out some finer points of electrophysiology with me, and Eleanore Hewitt for keeping our lab running smoothly.

Finally, and most significantly, I want to thank my friends and family, who helped keep up my morale throughout this process, especially my wife and best friend, Claire Whitner, who in her own words, felt as though she were constantly having to "tack Eeyore's tail back on".

The text and figures of Chapter I, in part, are a reprint of the material as it appears in: Mills RW, Narayan SM, McCulloch AD. The effects of wall stretch on ventricular conduction and refractoriness in the whole heart. In: Kohl P, Sachs F, Franz MR, eds. *Cardiac mechano-electric feedback and arrhythmias: From pipette to patient*. Philadelphia: Saunders/Elsevier; 2005:Chapter 14. Copyright © 2005 Elsevier Inc. Reprinted with permission from Elsevier. The dissertation author was the primary author and the co-authors listed in this publication directed and supervised.

The text and figures of Chapter II, in part, are a reprint of the material as it appears in: Sung D, Somayajula-Jagai J, Cosman P, Mills RW, McCulloch AD. Phase shifting prior to spatial filtering enhances optical recordings of cardiac action potential propagation. *Ann Biomed Eng*. 2001;29(10):854-861. Copyright © 2001 Biomedical Engineering Society. Reprinted with permission from Springer Science and Business Media. The dissertation author was the primary researcher and author of the work presented here, and the co-authors listed in this publication directed and supervised the research that forms the basis for this chapter, or were primary researchers of material *not* presented here.

The text and figures of Chapter III, in part, are a reprint of the material as it appears in: Sung D, Mills RW, Schettler J, Narayan SM, Omens JH, McCulloch AD. Ventricular filling slows epicardial conduction and increases action potential duration in an optical mapping study of the isolated rabbit heart. *J Cardiovasc Electrophysiol*. 2003;14(7):739-749. Copyright © 2003 Blackwell Futura Publishing Inc. Reprinted with permission from Blackwell Publishing. The disser-

tation author was the primary researcher and author of the work presented here, and the co-authors listed in this publication directed and supervised the research that forms the basis for this chapter, or were primary researchers of material *not* presented here.

The text of Chapter IV, in full, will be submitted for publication. The dissertation author was the primary researcher and author of the work presented here, and any co-authors of this publication directed and supervised the research that forms the basis for this chapter.

My first two years were supported by NIH Training Grant HL07089, my third year by NIH Training Grant HL07444, and my final three years by NSF Grant BES-0086482.

VITA

1977	Born, Ann Arbor, Michigan
1999	B.S. Biomedical Engineering, Johns Hopkins University Baltimore, Maryland
2000–2006	Research Assistant, University of California, San Diego
2001	M.S. Bioengineering, University of California, San Diego
2006	Ph.D. Bioengineering, University of California, San Diego

PUBLICATIONS

Sung D, Somayajula-Jagai J, Cosman P, **Mills RW**, McCulloch AD. Phase shifting prior to spatial filtering enhances optical recordings of cardiac action potential propagation. *Ann Biomed Eng.* 2001;29(10):854-861.

†Sung D, †**Mills RW**, Schettler J, Narayan SM, Omens JH, McCulloch AD. Ventricular filling slows epicardial conduction and increases action potential duration in an optical mapping study of the isolated rabbit heart. *J Cardiovasc Electrophysiol.* 2003;14(7):739-749. († co-first authors)

Mills RW, Narayan SM, McCulloch AD. The effects of wall stretch on ventricular conduction and refractoriness in the whole heart. In: Kohl, P, Sachs, F, Franz, MR, eds. *Cardiac mechano-electric feedback and arrhythmias: From pipette to patient*: Saunders/Elsevier; 2005:Chapter 14

Mills RW, Narayan SM, McCulloch AD. Mechanisms of Slowed Conduction During Ventricular Volume Loading (in preparation)

ABSTRACT OF THE DISSERTATION

Mechanisms of Slowed Conduction During Ventricular Volume Loading

by

Robert W. Mills
Doctor of Philosophy in Bioengineering
University of California, San Diego, 2006
Professor Andrew D. McCulloch, Chair

Several studies have linked increased myocardial strain (wall stretch) with atrial and ventricular arrhythmias. Although the precise mechanisms for these loading related rhythm disturbances remain unclear, the predominant mechanism underlying ventricular arrhythmias associated with mechanical dysfunction is reentrant conduction, which is promoted and sustained by slowed conduction. Passive ventricular volume loading in the Langendorff-perfused isolated rabbit heart has been shown to slow conduction.

Optical mapping was used to image myocardial conduction. A phase-shifting filtering technique was previously developed to enhance optical maps of myocardial electrical activity. The improvements of the phase-shifting scheme were validated by processing a known data set taken from a modified FitzHugh-Nagumo model, to which comparable noise was added. Further improvements were made to the filtering and analysis routines to improve efficiency and accuracy.

Conduction slowing in response to ventricular volume loading was validated by excluding several potentially confounding factors. Improved oxygen delivery with a synthetic oxygen carrier, indicated that the effect is not a result of

global ischemia. Measurement of regional tissue perfusion with microspheres suggested that the load effect is not due to regional ischemia. Conduction slowing was not significantly attributable to a decrease in epicardial surface temperature during loading. Measurements with epicardial electrodes were performed without two reagents used during optical mapping: di-4-ANEPPS and 2,3-butanedione monoxime. These measurements indicated that incremental loading within a physiological range still led to incrementally longer activation times (slowed conduction).

Several potential physiological mechanisms of conduction slowing during ventricular volume loading were investigated. Inclusion of the stretch-activated channel blocker gadolinium^{3+} in the perfusate attenuated the reversible increase in action potential duration during volume loading, but did not alter the reversible slowing of conduction. Volume loading reduced conduction despite changes in membrane excitability caused by varying perfusate potassium concentrations. Effective cross-fiber space and time constants, assessed by optical mapping of the tissue response to a cathodal-break point stimulus, increased significantly, indicating that loading may reduce intercellular resistance and increase effective membrane capacitance, resulting in a net slowing of conduction due to the greater sensitivity of conduction velocity to a change in capacitance.

Chapter I

General Introduction

Several studies have linked volume overload or increased myocardial strain (wall stretch) with atrial and ventricular arrhythmias. [1] Clinically, ventricular wall motion abnormalities, especially dyskinesia, [2] and congestive heart failure [3] are strongly related to arrhythmia, while abnormal increases in blood pressure result in ventricular hypertrophy that is linked with arrhythmic predisposition, [4] and which can be reduced by lowering blood pressure. [5] Experimentally, sudden increases in intraventriuclar pressure can induce arrhythmia even within normal physiological ranges. [6] Experimental models of heart failure, [7, 8] hypertrophy, [9, 10], and myocardial infarction [11] all show increased vulnerability to these load-induced arrhythmias. Further, it has been observed that reducing hypertrophy reduces arrhythmic susceptiblity [12].

Although the precise mechanisms for these mechanical load-induced rhythm disturbances remain unclear, they generally involve either triggered activity or reentrant conduction. [13] Mechanical stimuli in the intact heart can trigger ectopic activations or after-depolarizations, [14] and there is evidence that mechanical loading can create conditions necessary to initiate or maintain reentry. [15] Though both mechanisms may contribute, reentry is the predominant mechanism underlying ventricular arrhythmias associated with mechanical dysfunction [16] in patients with structural heart disease at risk for sudden cardiac death, [17] who

typically exhibit elevated filling pressures or wall motion abnormalities.

Reentry depends on the presence of excitable tissue ahead of the activation wavefront (an 'excitable gap') as it propagates around an area of structural or functional conduction block. Slowed conduction or decreased refractoriness can therefore promote and sustain reentry, while increased spatial and temporal *dispersion* of conduction velocity and refractoriness can provide a substrate for its initiation. [18] Ventricular wall strains measured during the cardiac cycle or as the result of altered hemodynamic loading display significant spatial heterogeneity. Since myocardial strain has been shown to modulate conduction velocity and refractory period, [18] altered mechanical loading may increase dispersion of conduction velocity and refractory period and thereby facilitate reentry. Observations on the acute effects of myocardial strain on conduction velocity have varied widely with experimental preparation, mechanical loading conditions and measurement techniques, while findings on the stretch-dependence of effective refractory period have been somewhat more consistent. Although there is compelling evidence that mechano-electric feedback influences myocardial conduction and refractoriness, more consistent quantitative data in the intact heart are still needed before a more definitive link to reentrant arrhythmia can be made. Given the inherent difficulties in measuring regional myocardial mechanics and conduction velocity in the whole heart without disturbing mechanical or electrical properties, many of the discrepancies between experimental reports are probably attributable to differences in experimental methods or definitions.

I.A The Effects Of Myocardial Stretch On Conduction Velocity

Conduction velocity is defined as the distance an activation wavefront travels per unit time (though 'distance' has several definitions - see below). Con-

duction velocity is not an intrinsic property, but rather a functional variable dependent on distributed cellular properties (e.g. membrane excitability and conduction resistances) and wavefront curvature, which influence the speed of impulse wave propagation; and is also dependent on myocardial tissue architecture, anisotropy, and stimulus sites, which influence conduction path. All of these factors are potentially affected by myocardial stretch, both physically, by changes in three-dimensional tissue, myocyte or membrane geometry, and physiologically, by mechanical regulation of ion channels and gap junctions or by mechanically triggered activity. The effect of stretch on conduction velocity *in vivo* is further complicated by the nonlinear, viscoelastic, anisotropic, time-varying, and heterogeneous mechanical properties of myocardium, and by the time-varying and heterogeneous myocardial stresses and strains.

I.A.1 Factors Influencing Conduction Speed

According to continuous cable theory, intracellular conduction is determined by passive membrane capacitance, longitudinal resistance, and voltage-dependent membrane conductances. [19] Membrane capacitance is a function of membrane dielectric properties and the membrane surface to cell volume ratio. An oncoming depolarization wavefront must first charge the membrane capacitance from resting to threshold, thus, increasing membrane capacitance will slow conduction. Intracellular and extracellular longitudinal resistances determine how rapidly ions travel in the direction of conduction, and are affected by the effective internal and external cross-sectional areas available for ion transport.

Above threshold, the voltage-gated fast sodium current usually determines how rapidly the local membrane depolarizes (action potential phase 0), creating the electrochemical gradient that drives longitudinal ion diffusion. These voltage-dependent conductances are influenced by channel kinetics and other regulatory processes, such as ligand gating and autonomic stimulation. [20] The integrated ability of ionic currents to depolarize the membrane and establish a longi-

tudinal potential gradient determines *membrane excitability*, which can be quantified by the rate of membrane depolarization at the onset of the action potential, Altering resting membrane potential influences conduction speed in a biphasic manner, [21] and model studies suggest that this effect acts through membrane excitability. [22] As resting membrane potential depolarizes, the difference between resting potential and sodium channel activation threshold potential decreases, requiring less membrane capacitive charging, thereby increasing conduction speed. Simultaneously, sodium channel inactivation increases with resting membrane depolarization, resulting in fewer channels available to open during activation, thus slowing conduction. The result of these competing effects is that a small depolarization of the membrane from normal rest potential increases conduction velocity, while a further depolarization slows conduction.

Within the electrically coupled syncytium, ionic movement between cells, and consequently myocardial conduction speed is modulated by the resistance of the gap junctions (1 - 5 MΩ). [23] However, though highly resistive, the effective resistance at normal levels of coupling is on the same order as that of the total myoplasmic resistance ($\sim$ 160 Ω-cm), and is significantly greater than the interstitial resistance ($\sim$ 60 Ω-cm). [24] Consequently, the degree of cellular coupling plays a significant role in determining myocardial conduction speed, [21] but must be significantly altered to significantly affect conduction speed. [25] Gap junction open probability is sensitive to ischemia, pH, intracellular magnesium and calcium, and transjunctional voltage. [26] While increased intercellular coupling speeds conduction, it also places a greater electrical load on depolarizing cells, as downstream cells draw away charge while their membrane capacitance is charging. Coupling to more downstream cells draws more charge, reducing the *safety factor* (ratio of charge source to charge sink) for propagation and thus increasing the risk of conduction block [27]. Activation wavefront curvature similarly affects propagation speed, as a convex wavefront must stimulate an expanding volume of resting tissue, imposing a greater electrical load and slowing conduction. [28]

Stretch may influence these determinants of conduction speed in several ways. Changes in cell geometry may alter membrane surface area and intracellular resistance. For example, uniaxial stretch along the fiber axis reduces myocyte cross-sectional area, and may thus decrease membrane surface area and hence specific membrane capacitance, which would speed conduction. However, fiber stretch also increases longitudinal resistance by increasing cell length and decreasing the cross-sectional area for current flow, thus slowing conduction. Stretch-activated ion currents may affect conduction velocity by altering resting potential and thus excitability. Studies in various preparations have demonstrated stretch-induced resting membrane depolarization to the point of activation threshold due to stretch that is blocked by gadolinium, consistent with the opening of cation non-selective stretch-activated channels. [29] It is not known whether acute mechanical stimuli alter gap junction permeability, but prolonged stretch in cell culture significantly upregulates connexin-43. [30]

I.A.2 Factors Influencing Conduction Path

Regional conduction speed is a reflection of the fastest conduction path through local myocardial architecture. Since the fastest conduction path to a region will activate that region, the resulting path of conduction is highly dependent on relative conduction speeds through different structures. Gap junctions are preferentially distributed at the ends of the cell aligned with the fiber axis. [26] Though lower cellular coupling in the cross-fiber direction results in less electrical load such that capacitance charging and action potential phase 0 are faster in the cross-fiber direction, conduction speed is typically 2 - 10 fold faster in the less resistive fiber direction. [19]

As the direction of fastest propagation follows the myocardial fiber direction, tissue conduction is anisotropic due to myocardial architecture. Conduction anisotropy is a function of cell shape, gap junction distributions, myocyte branching, fiber angle dispersion, and the laminar sheet organization of the myofibers

and the presence of connective tissue septa within the interstitium. Within the ventricle, fiber angles follow a left-handed helix in the epicardium and smoothly transition to a right-handed helix in the endocardium. Therefore, as activation spreads transmurally the principal axis of fastest in-plane propagation rotates and does not remain parallel to the fiber axis, and the wave front changes shape. Transverse to the fiber direction, cardiomyocytes are stacked into branching laminar sheets about 4 - 6 cells thick surrounded by a perimysial collagen fascia. A bidomain model based on a detailed three-dimensional reconstruction of tissue microarchitecture showed that this structural organization of the myocardium results in anisotropy transverse to the fibers, with conduction across the sheet planes being slowed by 40% compared with cross-fiber conduction within the sheets. [31] The local conduction speed, and consequently the overall path, will also be influenced by the distribution of ion channel isoforms between the different cell types within the endocardial, mid-myocardial, and epicardial regions. [32]

Since conduction is orthotropic with respect to fiber and sheet axes, strain can change the conduction path by altering local fiber and sheet directions. Stretch can also increase or decrease the dispersion of fiber and sheet angles about their mean directions, altering conduction speed and anisotropy. For example, Penefsky and Hoffman [33] suggest that increased fiber conduction velocity with stretch in isolated papillary muscles may have been associated with decreased fiber branching angles and dispersion as the muscles were elongated. This mechanism would also decrease cross-fiber conduction velocity if fiber stretch were greater than cross-fiber stretch, which is seen, for example, on the epicardium during passive filling. Shearing deformations in the wall, which are present whenever all directions do not stretch equally, can also change conduction anisotropy. For example, transverse torsional shearing during filling rotates the epicardium relative to the endocardium, and ventricular sphericalization during filling results in greater circumferential than longitudinal strain, [34] making epicardial and endocardial fibers more circumferential and decreasing transmural fiber angle gradients. This would increase cir-

cumferential speed, but decrease longitudinal speed. It has been reported that laminar myocardial sheets exhibit significant interlaminar shearing and rotation during early relaxation, [35] which may affect transmural conduction times and intramural electrotonic coupling.

I.A.3 Determinants of Regional Wall Stress and Strain

Myocardium and single myocytes are viscoelastic at rest, such that the response to a change in mechanical load or strain is history-dependent, [36] with a slow time constant of about 1000 seconds. [37] Many studies of myocardial mechano-electric feedback on conduction velocity accordingly have allowed several minutes for stabilization between load applications. Mechanical loading can therefore influence the observed electrophysiological effects of stretch, as different pressure or volume loading rates will result in different stresses or strains. Moreover, consecutive applications of the same load/unload cycle usually result in stress-strain relations that are more compliant at low strains, although these differences diminish with subsequent repetition, a process that is dominated by the *strain softening* property of myocardium. [37] Thus, more consistent stress-strain distributions between different load/unload cycles can be obtained with several *mechanical preconditioning* cycles, [36] which should also be more representative of myocardial conditions *in vivo*.

Myofilament activation also causes stress and strain to vary phasically throughout the cardiac cycle. [38] In studies of the effects of mechano-electric feedback on conduction velocity in the normal heart, diastolic mechanics are the most important determinant as electrical activation precedes systolic contraction, while at high heart rates when relaxation is incomplete, diastolic wall properties are influenced by myofilament interactions. At lower heart rates, afterload alterations have little direct influence on conduction velocity, but may significantly affect repolarization and refractoriness. Finally, cardiac geometry and fiber architecture strongly affect the local stress and strain distributions resulting from applied hemo-

dynamic loads. [38]

It remains unclear whether the effects of mechano-electric feedback correlate better with stress or strain. Changes in conduction path are determined by strain, but whether cellular responses are determined primarily by stress or strain depends fundamentally on the relative compliance of the molecular mechanotransducer, such as a stretch-activated ion channel. A membrane-spanning complex such as an ion channel is more likely to be sensitive to changes in stress than strain. The myocardial wall stress distribution is not readily measured, and is further complicated by *residual stress*, which is wall stress still present in the resting, unloaded heart. [38] Typically, a single scalar measure of wall stress is used, such as end-diastolic pressure, even though stress is a spatially varying three-dimensional tensor; such measurements complicate valid comparisons between geometries from different chambers or species. A complete description of myocardial strain requires the three-dimensional displacements of four or more non-coplanar markers, [39] so most investigators use incomplete one- or two-dimensional measurements, though three-dimensional strains have been measured using radiopaque markers [35] and MRI. [40] Ventricular strains tend to be regionally heterogeneous, though epicardial strain fields may be reasonably estimated from the displacements of arrayed epicardial surface markers. [41]

I.A.4 Measuring Conduction Velocity During Myocardial Stretch

In practice, conduction velocity is usually calculated in one dimension as the distance between recording electrodes aligned perpendicular to the wavepath divided by the interelectrode conduction time. During mechanical loading, the distance between recording sites and the number of myocytes per unit physical length can change. Thus, in the stretched state, conduction velocity may be defined on a cellular basis as the number of cells traversed per unit time, or more practically as the *unstretched* tissue length divided by the *stretched* segment conduction time (see Table I.1). When intercellular coupling sufficiently decreases, conduction time,

and hence velocity, becomes more dependent on the number of intercellular connections between the recording sites. In the extreme of discontinuous propagation, if strain had no other effect, then cellular conduction velocity would not change with stretch, and the material and spatial measures would increase, as fewer speed limiting intercellular resistances would be encountered per unit length.

Table I.1: Definitions Of Conduction Velocity In One Dimension:
$\Delta t(X)$ is the conduction time measured over interelectrode distance L_0 is the unstretched interelectrode distance, while L_1 is the stretched distance.

	Unstretched	Stretched
Cellular		$CV = \frac{L_0}{\Delta t\|_{L_1}}$
Spatial	$CV = \frac{L_0}{\Delta t\|_{L_0}}$	$CV = \frac{L_0}{\Delta t\|_{L_0}}$
Material		$CV = \frac{L_1}{\Delta t\|_{L_1}}$

In contrast, normal continuous conduction depends on the distribution of heterogeneous properties such as membrane capacitance and resistance. [19] Consequently, if stretch had no other effect, material and spatial conduction velocity would not change, and cellular velocity would decrease as conduction path length increased. Furthermore, conduction speed is dependent upon the specific distribution within the material segment measured, [33] thus, *material* conduction velocity describes how stretch affects the distribution of tissue properties that influence conduction velocity over a constant segment of tissue.

To make appropriate comparisons of conduction velocity before and during stretch, the material definition requires that the conduction path remains the same, which may not be accurate for conduction and stretch in more than one dimension. Consequently, in studies of two or three-dimensional conduction, a

highly resolved *spatial* description is most appropriate, as this description includes both differences in conduction speed due to changes in tissue properties, and differences in conduction direction due to changes in wavepath (see Figure I.1). In practice, to determine the two-dimensional conduction direction, the conduction time is sampled from an array of positions, from which isochrones of conduction time are generated, indicating the position of the activation wavefront. Conduction velocity is calculated as the distance traveled normal to the isochrones per unit time.

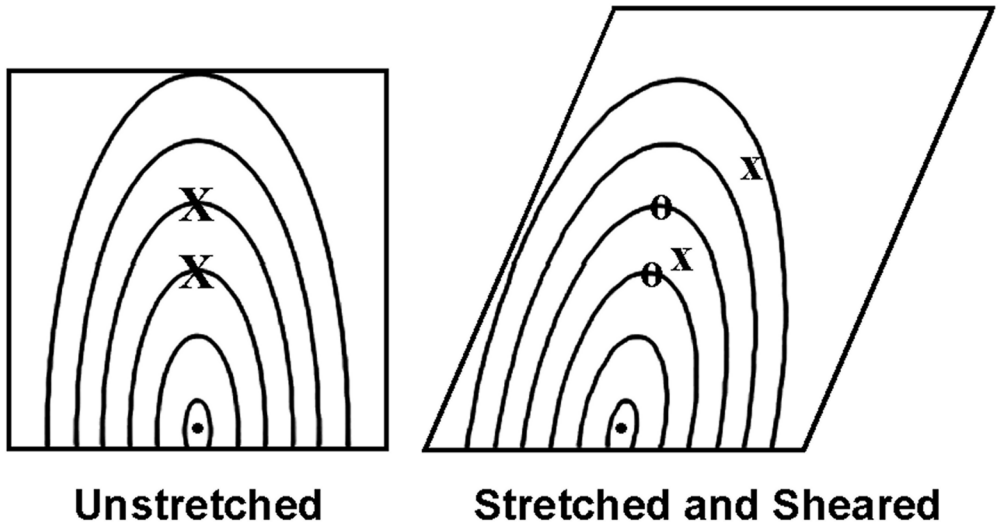

Figure I.1: Schematic of isochrones of activation due to pacing at •. 'X' indicates the initial position of recording electrodes, and 'x' indicates the electrode positions if the electrodes move with stretch, resulting in a material description of conduction velocity, but this is only correct if the measurement remains normal to the isochrones. However, conduction velocity calculated from any position and normal to the isochrones, as from '∘', is an exact, but spatial measure.

I.A.5 Effects of Stretch on Conduction Velocity in the Heart

Early investigations into the effects of myocardial stretch on conduction speed were limited to one-dimensional propagation. In studies of ventricular and atrial strips of myocardium from various species, stretching from slack length to the length of maximal developed tension caused a proportionate increase in spatial conduction velocity while material conduction velocity remained nearly unchanged. [33] Additional stretch, beyond the length of maximal developed tension, caused slowed propagation which was asynchronous between neighboring fibers, and a concurrent decrease in both spatial and material conduction velocity. The authors suggested that the initial increase in spatial conduction velocity with moderate stretch may be due to increased fiber alignment with stretch. Faster spatial conduction during stretch was also observed in sheep Purkinje fibers. [42, 43] In canine Purkinje fibers, both spatial and material conduction velocity initially increased with stretch and then decreased, but conduction in cat trabeculae was not similarly affected. [44] Conversely, spatial conduction velocity in rat papillary muscle decreased with stretch, while papillary muscle from several other species showed no effect. [45] Despite the varied effects of stretch across different structures, tissue types, and species, most of these studies imply that conduction velocity may increase with stretch. However, these studies mostly concentrated on specialized structures, and after being excised, these tissues were not subject to the same multiaxial constraints as *in vivo*.

Other studies have focused on the effect of physiological loading on whole chamber activation times. In the dog heart *in vivo*, QRS duration correlated with acute increases in left ventricular pressure, [46] while left atrial dilation increased atrial activation time, [47] and ventricular volume inflation in isolated rabbit hearts increased maximal activation times. [48] In contrast, one study of volume load in canine ventricle *in vivo* reported no change in spatial conduction time, [7] while cellular conduction velocity increased during volume load of rat atrium. [49] These whole chamber studies indicate that stretch slows material conduction, however,

possible changes in conduction path were not accounted for.

More recent studies have investigated the effects of stretch on two-dimensional epicardial surface conduction, in order to directly study the path of propagation. In volume-loaded left ventricle of isolated rabbit hearts after ventricular cryoablation of all but a thin epicardial layer, unloaded conduction velocities were estimated to be 76 $cm{\cdot}s^{-1}$ and 26 $cm{\cdot}s^{-1}$ in the fiber and cross-fiber directions, respectively. [50] Neither graded volume load nor decrements in pacing cycle length significantly altered these values. The authors acknowledged that the cryoablation procedure stiffened the ventricle, possibly protecting the viable layer from mechanical stimulus. Conversely, in right atrium of isolated rabbit hearts, balloon inflation caused an approximate 40% stretch in a nearly isotropic manner, and caused spatial conduction velocity to decrease from 73 $cm{\cdot}s^{-1}$ to 55 $cm{\cdot}s^{-1}$ at a cycle length of 250 ms. [51] In a similar study, an atrial filling pressure of 10.3 mmHg caused spatial conduction velocity to decrease by 3% from the control value of 65 $cm{\cdot}s^{-1}$ at a cycle length of 240 ms. [52] Atrial dilation caused a greater decrease in conduction velocity at shorter cycle lengths, increased the incidence of local functional conduction block (defined as conduction velocity less than 10 $cm{\cdot}s^{-1}$), increased conduction velocity dispersion, and altered the direction of propagation. Conduction velocity returned to normal after the pressure was removed.

Electrodes require physical contact with the myocardium possibly causing a local mechanical artifact. Sung et al. [53] used non-contact optical mapping during left ventricular volume loading in isolated rabbit heart, and employed a model-based analysis technique [54] that accounted for epicardial curvature and changes in conduction path, and allowed comparison of conduction velocity with local fiber direction. Intraventricular pressure was increased to 30 mmHg, which resulted in mean epicardial fiber strains on the order of 3% and mean cross-fiber strains near 1.5%, however, the distribution of these strains was regionally heterogeneous. [53] Figure I.2 shows an example of the increase in activation times due to

ventricular volume loading and the resulting velocity vector field. It also illustrates that application of stretch can alter the path of conduction. Spatial conduction velocity transverse to the fiber direction decreased on average by 16%, though spatial conduction velocity in the unloaded state near the pacing site (principally composed of epicardial conduction) was 20 $cm \cdot s^{-1}$, while distal to the pacing site (includes the more rapidly conducting endocardium) was on the order of 60 $cm \cdot s^{-1}$. Conduction velocity returned to baseline when load was removed.

These whole chamber studies that also include changes in conduction path consistently show conduction slowing due to stretch. The percent slowing of spatial conduction due to stretch was not proportional between atrial studies in which 40% strain caused 25% slowing, [51] while more than 23% strain caused 3% slowing [52] at nearly the same cycle length. This may indicate that conduction slowing is stress dependent in atrial tissue, as the passive stress-strain relation of biological tissues is similarly nonlinear. [38] Similarly, 1.5% epicardial cross-fiber strain at 30 mmHg caused 16% spatial conduction slowing in ventricle, [53] while greater than 23% strain at 9 mmHg caused 3% spatial slowing in atrium, [52] also implying that conduction slowing may correlate better with stress than strain.

I.A.6 Potential Interactions of Stretch with Factors that Influence Conduction Velocity

The effect of applied stretch on conduction velocity may be due to simple geometric or structural changes. Penefsky and Hoffman [33] postulated that increased one-dimensional spatial conduction velocity was the result of increased fiber alignment, and Deck [42] reasoned that stretch may reduce specific membrane capacitance (capacitance/area), though recent data suggest an increase of capacitance with stretch. [55] Similarly, Dominguez and Fozzard [43] suggested that stretch causes membrane unfolding (as recently confirmed [56]), decreasing membrane area per unit length without altering total membrane area, causing an apparent decrease in specific membrane capacitance. With a constant cell volume,

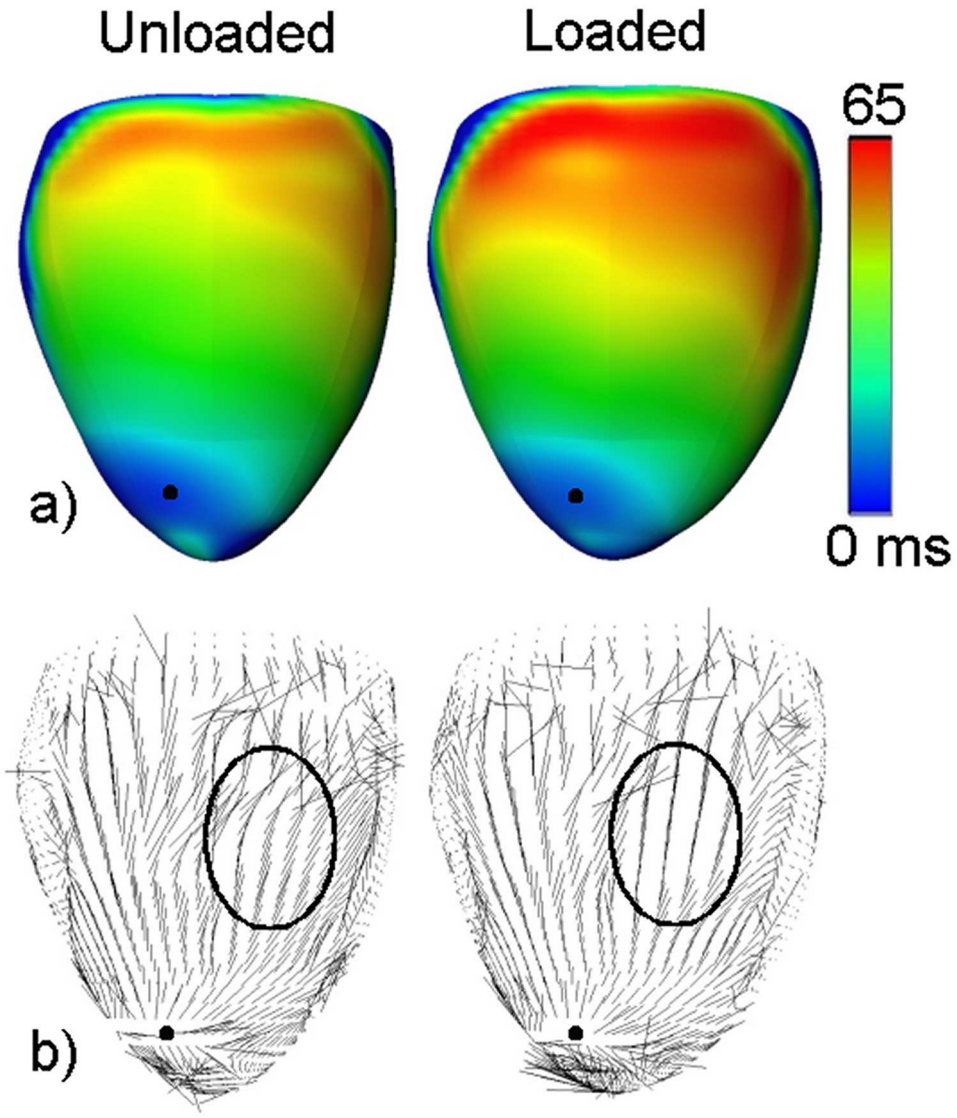

Figure I.2: Activation time fields (a) and conduction velocity vector fields (b) before and during application of 30 mmHg ventricular volume load in isolated rabbit heart, using methods from Sung et al. [53] The • indicates the approximate position of pacing. The ellipses outline a region in which the apparent direction of conduction has been changed by application of load.

fiber stretch will decrease cell cross-sectional area, also decreasing apparent specific membrane capacitance without changes in local membrane physical properties. However, this decrease in cell cross-sectional area would also increase longitudinal cytoplasmic resistance, thus *slowing* conduction. In canine Purkinje fibers, Rosen et al. [44] observed that stretch caused significant membrane unfolding and slightly increased packing of the extracellular space. These microstructural changes were accompanied by a biphasic increase then decrease in both spatial and material conduction velocity.

Stretch has also been reported to depolarize the resting membrane potential, [29] and this may be sufficient to slow conduction through fast sodium channel inactivation. Cation non-selective stretch-activated channels (SACs) have been reported with reversal potentials ranging from -70 to 30 mV, [57] and the resulting inward current depolarizes the resting membrane. Several of the effects of mechano-electric feedback in the whole heart have been seen to be blocked by non-specific inhibitors of SACs, including gadolinium inhibition of increased cellular conduction velocity during stretch in rat atria, [49] however, Sung et al. [53] observed that streptomycin did not affect the slowing of spatial conduction velocity during ventricular filling. Sustained stretch may also increase resting membrane potential through altered cellular calcium handling. [58] Myofilament binding sensitivity to calcium increases with stretch, and prolonged stretch results in a slow increase in the calcium transient, which subsequently interacts with other currents. However, increased resting potential should lower pacing threshold, but ventricular filling has been reported to have no effect on, [48, 59] or increase threshold. [50] SACs, altered calcium handling, or stretch-sensitive cellular signaling could also regulate the conductances associated with phase 0 of the action potential, thus decreasing the maximum rate of rise of membrane potential. [20]

Spear and Moore [45] suggested that stretch may increase intercellular resistance and slow conduction, and a heterogeneous or anisotropic reduction of coupling could also lead to changes in conduction path. Gap junction permeability

is regulated by several rapid factors, and has been observed to decrease within a few seconds after increases in intracellular sodium, magnesium, or especially calcium concentration. [26] Stretch may inhibit junctional conductance by increasing intracellular cation concentration through activation of stretch-activated channels or altered calcium handling. Gap junctions are also subject to slower cell signaling, specifically through phosphorylation by protein kinases A and C, which have been observed to both increase and decrease junctional permeability. [26] Stretch activation of these pathways could result in a decrease of intercellular conductance within one to three minutes.

Stretch may also reduce intercellular coupling by an independent mechanism. Though observed on myocyte lateral surfaces, cardiac gap junctions are primarily located in the intercalated discs along with the fascia adherens, which link the disc to the actin cytoskeleton, and desmosomes, which link to intermediate filaments. [60] Thus, most gap junctions co-localize with regions of maximum force transmission between cells, and may be modulated by these stresses. Moreover, junctional complexes tend to be located transverse to the fascia adherens. Consequently, longitudinal intercellular force transmission could subject gap junctions to a high degree of shear stress, and these stresses may effectively reduce electrical coupling between cells.

I.A.7 Summary

Conduction speed is functionally dependent on the distribution of heterogeneous properties including membrane excitability and cellular coupling, as well as activation wavefront curvature, while conduction path is functionally dependent upon regionally heterogeneous cellular and myocardial architectures. Evidence suggests that stretch affects conduction speed in various cardiac tissue types, and that the magnitude of conduction slowing in atrial and ventricular tissue is too great to be explained by physical changes in path length alone. Conduction slowing may be due to simple geometric and structural changes, though most of these

expected changes would tend to increase conduction velocity. Conduction could also be slowed due to decreased excitability through stretch-activated channel activation or length dependent calcium handling, but it is likely to be slowed in part by increased intercellular resistance.

I.B The Effect Of Myocardial Stretch On Effective Refractory Period

I.B.1 Determinants and Measurement of Effective Refractory Period

Effective refractory period (ERP) is the time interval following activation during which tissue is unable to activate again in response to the same stimulus, and thus is a measure of late-repolarization membrane excitability. ERP is determined by the voltage-regulated transition of fast sodium channels from the inactivated to the resting state, and is thus dependent on the time course of repolarization. Consequently, ERP is closely related to action potential duration (APD) and is also cycle-length dependent. One study observed that the ratio of ERP to monophasic APD at 90% recovery remains nearly constant despite a 60% decrease in action potential duration as cycle length decreases. [59] Effective refractory period is typically measured after continuous pacing at a single cycle length to minimize dynamic variations in action potential duration and other cellular kinetics. After this stabilization period, a stimulus is delivered at a shortened time delay (coupling interval). ERP is typically defined as the longest possible coupling interval that does not elicit a propagating action potential.

I.B.2 Effects of Stretch on Effective Refractory Period in Whole Heart

In-vivo studies of atrial mechano-electric feedback on effective refractory period have varied in their mechanical loading protocols. Ravelli [18] recently re-

viewed the effect of stretch on ERP in atrial myocardium, and attributed most variations to differences in timing and duration of stretch, as seen in model studies, [61] but attributed some differences to homeostatic regulation *in vivo* or possible species differences. Despite these variations, studies have consistently shown that acute atrial stretch increases the dispersion of effective refractory periods.

Recent canine studies show that effective refractory period increases when stretching isolated canine right atrium [62] or canine left ventricle *in vivo* via volume load. [7] These observations are consistent with most previous canine studies, though ERP shortening has been observed during volume inflation of canine atrium. [47] However, in rabbit atria, increasing pressure consistently and reversibly *shortens* ERP, suggesting a possible species specificity. At a drive cycle length of 250 ms, ERP has been shown to shorten from approximately 80 ms to 50 ms following an increase of approximately 15 cm H_20 of atrial pressure or an increase in atrial length of 40%. [51, 63, 64, 65]

Studies on the effects of stretch on left *ventricular* effective refractory period have been more consistent across different species and experimental methods. In swine heart *in vivo*, an increase in afterload caused a greater decrease in ERP at the apex than the base, thus increasing dispersion of refractoriness. [66] Similarly, in studies of isolated rabbit heart, left ventricular volume loading [48] or increased preload [67] also decreased ERP. Increased preload decreased ERP in a manner that correlated better with increased diastolic wall stress, as estimated from end diastolic pressure and ventricular geometry, than with increased systolic wall stress or diastolic circumference. Dilation also shortened ERP more significantly on the endocardial than epicardial surface. [59] This indicates that ERP may correlate better with cross-fiber than fiber stress or strain, since myocardial residual stress and torsion during filling allow a more uniform transmural distribution of fiber strain [38] under load at the expense of cross-fiber strain gradients.

In rabbit, ventricular stretch caused by increasing preload also caused greater shortening of effective refractory period as the drive cycle length

decreased. [50] This finding was later corroborated in isovolumically contracting rabbit ventricles. [59] Reiter et al. [50] suggest that this rate dependency may follow dependency on the stretch-sensitive delayed rectifier potassium current.

Those studies that also examined the effect of stretch on action potential duration observed that mechano-electric feedback on late APD (typically 90% recovery) reflected the observed effects on effective refractory period, either increasing [7] or decreasing [48, 59, 63, 66] with stretch in atria and ventricles, and did not alter the ratio of ERP to late APD. [59] Several other studies have reported a decrease in late action potential duration with stretch in various species including lamb, swine, guinea pig, rabbit, and human. However, some investigators report an *increase* in late APD during stretch in canine and other species consistent with a cation non-selective stretch-activated channel, and presumably, ERP would reflect this increase. Nilius and Boldt [68] observed a lengthening of APD at 90% recovery (APD_{90}) with stretch in rabbit atrial trabeculae that they attributed to a decreased potassium current near resting potential. Volume loading of the left atrium in guinea pig variably affected both APD_{50} and APD_{90}, with about a quarter of observed APD's increasing during stretch. [69] In contrast, axial stretch of isolated guinea pig ventricular myocytes caused a consistent prolongation of APD_{20}, APD_{50}, and APD_{90}. Similarly, volume loading of isolated rabbit ventricle caused an increase in APD_{20} and APD_{80}. [53] These studies indicate that in some non-canine preparations, ERP may *increase* with stretch. Finally, several studies by the Franz group also observe late APD lengthening in canine and rabbit, but see it shortening at earlier levels of recovery. [29] Franz suggests that depending on the stimulus strength used, mechano-electric feedback on ERP may simply reflect changes in APD at varying levels, thus, ERP could shorten during stretch reflecting shortening of early APD, while late APD lengthens.

I.B.3 Potential Interactions of Stretch with Factors that Influence Effective Refractory Period

Stretch-activated channels (SACs) and altered calcium handling have both been implicated in stretch-induced action potential duration shortening, [18] and consequently could influence effective refractory period. Model studies indicate that the effect of stretch can have various influences on action potential shape depending on the relative contributions of SACs and calcium handling, both of which are sensitive to timing and intensity of stretch. [61, 70] Zabel et al. [70] showed that including a length dependent non-specific cationic conductance with a reversal potential near -30 mV could reproduce several experimental observations including early APD shortening and late APD lengthening during stretch, while Kohl [61] showed that a more moderate stretch can lead to an overall shortening of APD. Kohl further showed that stretch in a model that included sarcomere length-dependent calcium handling would produce an overall prolongation of APD if applied early or sustained throughout the action potential, but an overall shortening if applied during late repolarization.

Investigations into the mechanisms of stretch-induced effective refractory period shortening by pharmacological interventions have yielded inconsistent results. Streptomycin, a blocker of cationic stretch-activated channels, inhibited acute stretch-induced shortening of rabbit ventricular ERP, but had no effect during sustained stretch. [59] In contrast, the more specific SAC blocker GsMtx-4 did not block stretch-induced shortening of rabbit atrial ERP, although this may have been be due to resistance of the potassium selective SAC to these compounds. [65] Zarse et al. [64] found that the L-type calcium channel blocker verapamil inhibited stretch-induced shortening of atrial ERP, suggesting the contribution of a length-dependent calcium handling mechanism, [58] but others have observed no effect of verapamil on rabbit ventricular ERP shortening. [59]

Increased dispersion of effective refractory period with stretch may follow inhomogeneous stress or strain distributions. A ventricular model study that

coupled physiological fiber and cross-fiber strains to a stretch-dependent current within an action potential model predicted a near doubling of the dispersion of late APD. [71] Finally, a reduction in cellular coupling could lead to greater heterogeneity of repolarization as the electrical activity of individual cells becomes more independent.

I.B.4 Summary

Increased preload, afterload, or sustained load typically decreases effective refractory period, however, ERP follows action potential duration, and some have observed APD prolongation at all levels of recovery. How stretch effects ERP is likely a result of the balance of several competing effects including stretch-activated channels that can be cation selective or K^+ selective, altered calcium handling, and the timing and intensity of stretch, which could have varying levels of activation in different species and manners of stretch.

I.C Conclusions

Recent evidence provides a basis to explain why stretch is associated with arrhythmias, particularly reentrant forms. Both atrial and ventricular stretch slow spatial conduction, while atrial stretch increases conduction velocity dispersion and increases the occurrence of local functional conduction block, all of which promote reentrant arrhythmias. These stretch effects may correlate with the application of diastolic mechanical load, but correlation with stress or strain is less clear owing to regionally heterogeneous cardiac geometry, structure, and time-dependent material properties. Stretch may affect conduction velocity through reduced effective cellular coupling, cellular level geometric changes, or alterations in excitability, particularly an increase in resting membrane potential due to the activity of stretch-activated channels or altered calcium handling.

In general, both atrial and ventricular stretch decrease effective refractory period, but stretch consistently increases dispersion of effective refractory period, both of which are associated with increased incidence of reentrant arrhythmias. The effects of stretch on refractoriness parallel effects on action potential duration, which may vary as a function of the relative activation of competing mechanisms, including stretch-activated channels and altered calcium handling.

I.D Objectives Of The Dissertation

The primary objective of this dissertation is to investigate the mechanisms that could contribute to the slowing of conduction during left-ventricular volume loading. These studies were separated into two aspects: those possible mechanisms that were experimental methodology dependent, and those mechanisms that would reflect real cellular regulation or biophysical phenomena.

The first specific aim of this dissertation was to further develop and validate the signal-processing and analysis algorithms used to obtain measurements of conduction velocity from optical maps of apparent epicardial conduction in the Langendorff-perfused isolated rabbit heart preparation during varied volume loading. This involved validation with simulated data to which noise was added, and extension of the signal processing routines to handle large quantities of data in an efficient and accurate manner. These aspects are covered in Chapter II.

The second specific aim of this dissertation was to investigate the contributions of potential confounding factors in the experimental methodology, including loading associated ishemia or hypothermia, the use of the excitation-contraction uncoupler, 2,3-butanedione monoxime, used to inhibit motion artifact in the optical signals, and the use of the voltage-sensitive dye, di-4-ANEPPS, used to acquire the optical maps. These studies are described in Chapter III.

The final specific aim of this dissertation was to investigate the poten-

tial mechanisms of conduction slowing due to loading associated regulation of ion conductances or loading associated modification of the biophysics of the electrical syncytium of the myocardium. These studies are described in Chapter IV.

The text and figures of this chapter, in part, are a reprint of the material as it appears in: Mills RW, Narayan SM, McCulloch AD. The effects of wall stretch on ventricular conduction and refractoriness in the whole heart. In: Kohl P, Sachs F, Franz MR, eds. *Cardiac mechano-electric feedback and arrhythmias: From pipette to patient.* Philadelphia: Saunders/Elsevier; 2005:Chapter 14. The dissertation author was the primary author and the co-authors listed in this publication directed and supervised.

References

[1] Stevenson WG, Stevenson LW. Prevention of sudden death in heart failure. *J Cardiovasc Electrophysiol*. 2001;12(1):112-114.

[2] Siogas K, et al. Segmental wall motion abnormalities alter vulnerability to ventricular ectopic beats associated with acute increases in aortic pressure in patients with underlying coronary artery disease. *Heart*. 1998;79(3):268-273.

[3] Reiter MJ. Effects of mechano-electrical feedback: Potential arrhythmogenic influence in patients with congestive heart failure. *Cardiovasc Res*. 1996;32(1):44-51.

[4] Pringle SD, et al. Significance of ventricular arrhythmias in systemic hypertension with left ventricular hypertrophy. *Am J Cardiol*. 1992;69(9):913-917.

[5] Sideris DA. High blood pressure and ventricular arrhythmias. *Eur Heart J*. 1993;14(11):1548-1553.

[6] Hansen DE, Craig CS, Hondeghem LM. Stretch-induced arrhythmias in the isolated canine ventricle. Evidence for the importance of mechanoelectrical feedback. *Circulation*. 1990;81(3):1094-1105.

[7] Zhu WX, et al. Impact of volume loading and load reduction on ventricular refractoriness and conduction properties in canine congestive heart failure. *J Am Coll Cardiol*. 1997;30(3):825-833.

[8] Pye MP, Cobbe SM. Arrhythmogenesis in experimental models of heart failure: The role of increased load. *Cardiovasc Res*. 1996;32(2):248-257.

[9] Wang Z, et al. Initiation of ventricular extrasystoles by myocardial stretch in chronically dilated and failing canine left ventricle. *Circulation*. 1994;90(4):2022-2031.

[10] Jauch W, Hicks MN, Cobbe SM. Effects of contraction-excitation feedback on electrophysiology and arrhythmogenesis in rabbits with experimental left ventricular hypertrophy. *Cardiovasc Res*. 1994;28(9):1390-1396.

[11] Calkins H, et al. Effect of acute volume load on refractoriness and arrhythmia development in isolated, chronically infarcted canine hearts. *Circulation*. 1989;79(3):687-697.

[12] Schmieder RE, Messerli FH. [ventricular arrhythmia and sudden cardiac death: The significance of left ventricular hypertrophy as risk factor]. *Schweiz Med Wochenschr*. 1993;123(4):99-107.

[13] Taggart P, Sutton PM. Cardiac mechano-electric feedback in man: Clinical relevance. *Prog Biophys Mol Biol*. 1999;71(1):139-154.

[14] Franz MR, et al. Mechanically induced action potential changes and arrhythmia in isolated and in situ canine hearts. *Cardiovasc Res.* 1989;23(3):213-223.

[15] Cabo C, Wit AL. Cellular electrophysiologic mechanisms of cardiac arrhythmias. *Cardiol Clin.* 1997;15(4):517-538.

[16] Kuo CS, et al. Characteristics and possible mechanism of ventricular arrhythmia dependent on the dispersion of action potential durations. *Circulation.* 1983;67(6):1356-1367.

[17] Myerburg RJ. Scientific gaps in the prediction and prevention of sudden cardiac death. *J Cardiovasc Electrophysiol.* 2002;13(7):709-723.

[18] Ravelli F. Mechano-electric feedback and atrial fibrillation. *Prog Biophys Mol Biol.* 2003;82(1-3):137-149.

[19] Kootsey JM. Electrical propagation in distributed cardiac tissue. In: Glass L, Hunter P, McCulloch AD, eds. *Theory of heart: Biomechanics, biophysics, and nonlinear dynamics of cardiac function.* New York: Springer-Verlag; 1991:391-403.

[20] Roden DM, et al. Cardiac ion channels. *Annu Rev Physiol.* 2002;64431-475.

[21] Rohr S, Kucera JP, Kleber AG. Slow conduction in cardiac tissue, i: Effects of a reduction of excitability versus a reduction of electrical coupling on microconduction. *Circ Res.* 1998;83(8):781-794.

[22] Nygren A, Giles WR. Mathematical simulation of slowing of cardiac conduction velocity by elevated extracellular [k+] in a human atrial strand. *Ann Biomed Eng.* 2000;28(8):951-957.

[23] Weingart R. Electrical properties of the nexal membrane studied in rat ventricular cell pairs. *J Physiol.* 1986;370267-284.

[24] Kleber AG, Riegger CB. Electrical constants of arterially perfused rabbit papillary muscle. *J Physiol.* 1987;385307-324.

[25] Thomas SP, et al. Impulse propagation in synthetic strands of neonatal cardiac myocytes with genetically reduced levels of connexin43. *Circ Res.* 2003;92(11):1209-1216.

[26] Dhein S. *Cardiac gap junctions.* New York: Karger; 1998.

[27] Rudy Y. The ionic mechanisms of conduction in cardiac tissue. *J Electrocardiol.* 2001;34 Suppl65-68.

[28] Cabo C, et al. Wave-front curvature as a cause of slow conduction and block in isolated cardiac muscle. *Circ Res.* 1994;75(6):1014-1028.

[29] Franz MR. Mechano-electrical feedback in ventricular myocardium. *Cardiovasc Res.* 1996;32(1):15-24.

[30] Zhuang J, et al. Pulsatile stretch remodels cell-to-cell communication in cultured myocytes [see comments]. *Circulation Research.* 2000;87(4):316-322.

[31] Hooks DA, et al. Cardiac microstructure: Implications for electrical propagation and defibrillation in the heart. *Circ Res.* 2002;91(4):331-338.

[32] Jalife J, Anumonwo JM, Berenfeld O. Toward an understanding of the molecular mechanisms of ventricular fibrillation. *J Interv Card Electrophysiol.* 2003;9(2):119-129.

[33] Penefsky ZJ, Hoffman BF. Effects of stretch on mechanical and electrical properties of cardiac muscle. *Am J Physiol.* 1963;204(3):433-438.

[34] Omens JH, MacKenna DA, McCulloch AD. Measurement of strain and analysis of stress in resting rat left ventricular myocardium. *J Biomech.* 1993;26(6):665-676.

[35] Ashikaga H, et al. Transmural left ventricular mechanics underlying torsional recoil during relaxation. *Am J Physiol Heart Circ Physiol.* 2004;286(2):H640-647.

[36] Fung YC. *Biomechanics : Mechanical properties of living tissues.* 2nd ed. ed. New York: Springer-Verlag; 1993.

[37] Emery JL, Omens JH, McCulloch AD. Strain softening in rat left ventricular myocardium. *J Biomech Eng.* 1997;119(1):6-12.

[38] McCulloch AD, Omens JH. Factors affecting the regional mechanics of the diastolic heart. In: Glass L, Hunter P, McCulloch AD, eds. *Theory of heart: Biomechanics, biophysics, and nonlinear dynamics of cardiac function.* New York: Springer-Verlag; 1991:87-119.

[39] Waldman LK, Fung YC, Covell JW. Transmural myocardial deformation in the canine left ventricle. Normal in vivo three-dimensional finite strains. *Circ Res.* 1985;57(1):152-163.

[40] Faris OP, et al. Novel technique for cardiac electromechanical mapping with magnetic resonance imaging tagging and an epicardial electrode sock. *Ann Biomed Eng.* 2003;31(4):430-440.

[41] Mazhari R, et al. Regional myocardial perfusion and mechanics: A model-based method of analysis. *Ann Biomed Eng.* 1998;26(5):743-755.

[42] Deck KA. [changes in the resting potential and the cable properties of purkinje fibers during stretch]. *Pflugers Arch Gesamte Physiol Menschen Tiere.* 1964;280131-140.

[43] Dominguez G, Fozzard HA. Effect of stretch on conduction velocity and cable properties of cardiac purkinje fibers. *Am J Physiol*. 1979;237(3):C119-124.

[44] Rosen MR, Legato MJ, Weiss RM. Developmental changes in impulse conduction in the canine heart. *Am J Physiol*. 1981;240(4):H546-554.

[45] Spear JF, Moore EN. Stretch-induced excitation and conduction disturbances in the isolated rat myocardium. *J Electrocardiol*. 1972;5(1):15-24.

[46] Sideris DA, et al. Effect of acute ventricular pressure changes on qrs duration. *J Electrocardiol*. 1994;27(3):199-202.

[47] Solti F, et al. The effect of atrial dilatation on the genesis of atrial arrhythmias. *Cardiovasc Res*. 1989;23(10):882-886.

[48] Zabel M, Portnoy S, Franz MR. Effect of sustained load on dispersion of ventricular repolarization and conduction time in the isolated intact rabbit heart. *J Cardiovasc Electrophysiol*. 1996;7(1):9-16.

[49] Tavi P, Laine M, Weckström M. Effect of gadolinium on stretch-induced changes in contraction and intracellularly recorded action- and afterpotentials of rat isolated atrium. *British Journal of Pharmacology*. 1996;118(2):407-413.

[50] Reiter MJ, et al. Electrophysiological effects of acute dilatation in the isolated rabbit heart: Cycle length-dependent effects on ventricular refractoriness and conduction velocity. *Circulation*. 1997;96(11):4050-4056.

[51] Chorro FJ, et al. [acute changes in wavelength of the process of auricular activation induced by stretching. Experimental study]. *Rev Esp Cardiol*. 1998;51(11):874-883.

[52] Eijsbouts SC, et al. Effects of acute atrial dilation on heterogeneity in conduction in the isolated rabbit heart. *J Cardiovasc Electrophysiol*. 2003;14(3):269-278.

[53] Sung D, et al. Ventricular filling slows epicardial conduction and increases action potential duration in an optical mapping study of the isolated rabbit heart. *J Cardiovasc Electrophysiol*. 2003;14(7):739-749.

[54] Sung D, Omens JH, McCulloch AD. Model-based analysis of optically mapped epicardial activation patterns and conduction velocity. *Ann Biomed Eng*. 2000;28(9):1085-1092.

[55] Suchyna TM, Besch SR, Sachs F. Dynamic regulation of mechanosensitive channels: Capacitance used to monitor patch tension in real time. *Physical Biology*. 2004;1(1):1-18.

[56] Kohl P, Cooper PJ, Holloway H. Effects of acute ventricular volume manipulation on in situ cardiomyocyte cell membrane configuration. *Prog Biophys Mol Biol.* 2003;82(1-3):221-227.

[57] Hu H, Sachs F. Stretch-activated ion channels in the heart. *J Mol Cell Cardiol.* 1997;29(6):1511-1523.

[58] Calaghan SC, Belus A, White E. Do stretch-induced changes in intracellular calcium modify the electrical activity of cardiac muscle? *Prog Biophys Mol Biol.* 2003;82(1-3):81-95.

[59] Eckardt L, et al. Modification of stretch-induced shortening of repolarization by streptomycin in the isolated rabbit heart. *J Cardiovasc Pharmacol.* 2000;36(6):711-721.

[60] Gutstein DE, et al. The organization of adherens junctions and desmosomes at the cardiac intercalated disc is independent of gap junctions. *J Cell Sci.* 2003;116(Pt 5):875-885.

[61] Kohl P, Day K, Noble D. Cellular mechanisms of cardiac mechanoelectric feedback in a mathematical model. *Canadian Journal of Cardiology.* 1998;14(1):111-119.

[62] Huang JL, et al. Effect of atrial dilatation on electrophysiologic properties and inducibility of atrial fibrillation. *Basic Res Cardiol.* 2003;98(1):16-24.

[63] Ravelli F, Allessie M. Effects of atrial dilatation on refractory period and vulnerability to atrial fibrillation in the isolated langendorff-perfused rabbit heart. *Circulation.* 1997;96(5):1686-1695.

[64] Zarse M, et al. Verapamil prevents stretch-induced shortening of atrial effective refractory period in langendorff-perfused rabbit heart. *J Cardiovasc Electrophysiol.* 2001;12(1):85-92.

[65] Bode F, Sachs F, Franz MR. Tarantula peptide inhibits atrial fibrillation. *Nature.* 2001;409(6816):35-36.

[66] Dean JW, Lab MJ. Regional changes in ventricular excitability during load manipulation of the in situ pig heart. *J Physiol.* 1990;429387-400.

[67] Halperin BD, et al. Mechanical correlates of contraction-excitation feedback during acute ventricular dilatation. *Cardiovasc Res.* 1993;27(6):1084-1087.

[68] Nilius B, Boldt W. Stretching-induced changes in the action potential of the atrial myocardium. *Acta Biol Med Ger.* 1980;39(2-3):255-264.

[69] Babuty D, Lab M. Heterogeneous changes of monophasic action potential induced by sustained stretch in atrium. *J Cardiovasc Electrophysiol.* 2001;12(3):323-329.

[70] Zabel M, et al. Stretch-induced voltage changes in the isolated beating heart: Importance of the timing of stretch and implications for stretch-activated ion channels. *Cardiovascular Research*. 1996;32(1):120-130.

[71] Vetter FJ, McCulloch AD. Mechanoelectric feedback in a model of the passively inflated left ventricle. *Ann Biomed Eng*. 2001;29(5):414-426.

Chapter II

Analytical Methods for Optical Mapping Data

II.A Abstract

Using charge-coupled devices to optically map myocardial electrical activity offers several advantages, but these devices tend to have low signal-to-noise ratios. We previously developed a phase-shifting filtering technique to improve signal-to-noise while preserving the upstroke of the action potential, but this technique comes at computational expense. The improvements of the phase-shifting scheme were validated by processing a known data set taken from a modified FitzHugh-Nagumo model, to which comparable noise was added. Further improvements were made to the filtering and analysis routines to improve efficiency and accuracy.

II.B Introduction

Optical mapping is frequently used for studying mechano-electric feedback, as this technique of recording myocardial electrical activity does not require

physical contact with the myocardium, as compared to other methods, such as monophasic action potentials, surface electrograms, and microelectrodes, which may introduce mechanical artifact. [1] Optical mapping can achieve higher spatial resolution that most conventional electrode arrays, [2] is a measure of transmembrane voltage rather than extracellular potential, [3] and has been shown to have excellent correlation with microelectrode recordings of action potentials. [4] In comparison to optical techniques, multi-electrode arrays can equally assess activation, but only monophasic action potential and microelectrode techniques can reliably assess local transmembrane activity and repolarization, and these techniques are not practical for high-resolution multi-site mapping. [2]

Of the currently available technologies for acquisition of the fluorescent signal emitted from the potentiometric dyes used in optical mapping, charge-coupled devices (CCD) tend to have several advantages over photodiode arrays (PDA) and complementary metal-oxide semiconductor (CMOS) cameras. CCD devices tend to have higher spatial resolution than PDAs, and currently tend to have better dynamic range to CMOS cameras, making them superior in low light applications. However, CCD cameras tend to have lower temporal resolution, and poorer signal-to-noise ratios.

To improve measurements of activation time (and consequently conduction velocity) and repolarization time from CCD recordings of myocardial electrical activity, we previously developed a combined spatial and temporal filtering technique that improves signal-to-noise of optically recorded action potentials. Spatial filtering uses the weighted mean of a small neighborhood of adjacent pixels, but since ectopically elicited activation propagates electrical activity in a wave-like manner through a highly-coupled syncytium, adjacent pixels record morphologically similar but phase-offset signals. This offset potentially introduces a temporal error into the spatially filtered signals, especially within the quickly rising action potential upstroke. Consequently, the filtering technique was further developed to include phase-correction shifting prior to weighted spatial averaging. [5]

Implementation of this technique greatly increased the computational overhead in filtering typical data sets. A stack of 120 images (a single optical action potential and surrounding resting potential signal) required 160 minutes to filter with phase-shifting, while requiring only 4 minutes without. Further, a typical data set of 2 seconds of imaging contains roughly 5 action potentials, which must be manually parsed and individually filtered, as several filtering routines relied on being presented with single action potentials. In addition, basic analysis algorithms can be sensitive to irregularities in morphology. The objective of this work was to validate the utility of the phase-shifting algorithm in light of its increase in computational expense, and to reduce the number of man and computational hours required by re-implementing these data processing routines as necessary to create autonomous and efficient filtering and robust analysis algorithms in light of the approximate 150 - 300 propagating optical potentials to be analyzed per study.

II.C Experimental Methods

II.C.1 Isolated Heart Preparation and Experimental Protocol

All data were acquired from isolated Langendorff-perfused rabbit heart preparations as previously described [6] under animal use protocols approved by the UCSD Institutional Animal Care and Use Committee. Briefly, the heart was isolated and retrogradely perfused with warmed(35° - 37°C) and oxygenated (95% O_2, 5% CO_2) modified Tyrode's solution composed of: 130 mM NaCl, 4.5 mM KCl, 1.3 mM $CaCl_2$, 1.1 mM $MgCl_2$, 25 mM $NaHCO_3$, 1.2 mM NaH_2PO_4, 10.0 mM dextrose. Surface ECG and total coronary inflow were continuously monitored. The heart was apically paced at twice diastolic threshold at a cycle length of 360 ms.

II.C.2 Optical Mapping

Optical mapping was performed as previously described. [6] Briefly, after staining with a 10 mL bolus of the voltage-sensitive dye, di-4-ANEPPS (10.4 μM), the dye was excited at 516 $\pm$ 45 nm from a 300 Watt xenon arc lamp. Epifluorescence was passed through a $>$ 610 nm filter and focused with a high numerical aperture lens (f/0.95, Navitar, Rochester, NY) onto an 8-bit CCD camera (Dalsa, Waterloo, Ontario model CA-D1-256) at 399 frames/second and a resolution of 128 $\times$ 126 pixels, imaging an approximate 9-cm^2 area. Additional 5 mL dye injections were given as needed to maintain acquired fluorescent signal intensity. The electromechanical uncoupling agent 2,3-butanedione monoxime (BDM, 12.5 mM) was added to a secondary perfusate reservoir, which was used to perfuse the heart during data acquisition, and was washed out immediately after data acquisition.

II.D Validation of Phase-Shift Filtering

II.D.1 Methods

To quantify the effects of the signal processing scheme on signal accuracy, a propagating action potential was simulated using a modified FitzHugh-Nagumo model. [7] A 16 $\times$ 32 finite element mesh was constructed representing a 5 $\times$ 10 mm rectangle of tissue. The model was sampled at 500 Hz at the nodes, giving a spatial and temporal resolution comparable to those used in experiments. The diffusion coefficients were set to give an approximate conduction velocity of 20 cm/s in the cross-fiber direction and 30 cm/s in the fiber direction, which are within the ranges observed in experiments. This combination of parameters resulted in a phase shift between nodes of 1.0 - 1.5 ms, which is comparable to the range seen in experiments (0.4 - 1.6 ms), resulting in a range of phase shifts within a pixel neighborhood that was similar to or greater than the sampling period of 2 ms.

The signals were scaled to cover a range of 15, which is similar to the range of the measured 8-bit intensity valued optical action potentials. Gaussian noise ($\sigma = 0.7$) was independently added to each signal, after which the signals were rounded to the nearest integer, resulting in quantized noisy signals like those observed in experiments. The signals were then rescaled to a range of 6, corresponding to the range of experimental signals after normalization (Figure II.1). This data set was then filtered using the phase-shifting algorithm.

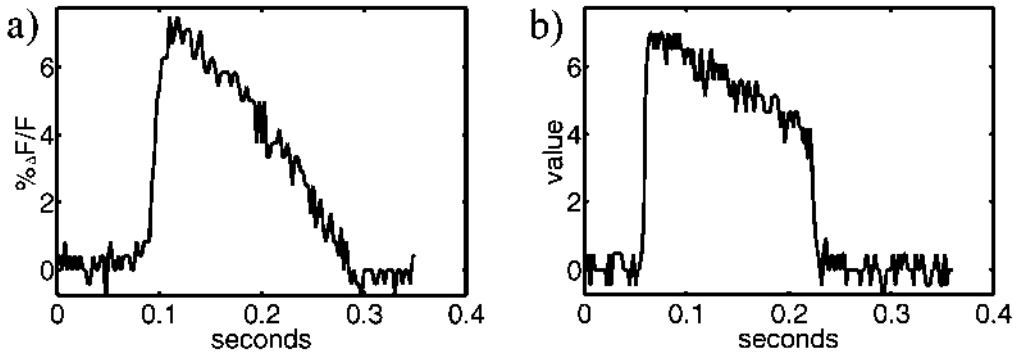

Figure II.1: (a) Representative acquired raw signal after inversion and normalization and (b) a representative generated raw signal before filtering.

Four error measures were used to evaluate signal quality. These error measures were all percent differences between the final filtered signal and the original simulated signal (before noise had been added), specifically: (1) percent mean signed difference of the rate of depolarization, calculated by sequence averaging the difference of the rate of depolarization throughout the upstroke for each signal, and dividing by the ensemble average of the maximum rate of depolarization; (2) percent mean absolute difference of the signal magnitude during repolarization, calculated by sequence averaging the absolute difference of the signal throughout repolarization (signal peak to 80% recovery), then dividing by the ensemble average

of the maximum signal magnitude (during repolarization); (3 and 4) percent signed difference of activation and repolarization times (as determined by the feature extraction algorithm described above), calculated by taking the signed difference for each signal, and dividing by the ensemble average of action potential duration (as defined above).

II.D.2 Results

Table II.1 shows the distribution statistics of the above error measures calculated from the application of three different Gaussian convolution kernels: 3×3 ($\sigma = 0.631$), 5×5 ($\sigma = 1.179$), and 7×7 ($\sigma = 1.475$) with and without phase correction. Without the phase correction, the 3×3 filter resulted in a modest improvement in signal quality, as seen in the decrease of depolarization rate error deviation, repolarization error, and repolarization error deviation. Application of the larger sized filters decreased repolarization error and deviation, but worsened depolarization rate error and deviation due to blurring from averaging over a larger area, which compounds slight errors in phase alignment due to signal discretization in time. Incorporating the phase correction improved signal quality compared to the non-phase corrected for all three kernel sizes. The phase correction significantly decreased the depolarization rate error and deviation. The decrease in signed error indicates that the algorithm attenuates a systematic error that reduces measured upstroke rate when filtering without phase correction. The effect on signal-to-noise ratio due to phase correction was not appreciable. Phase correction also removes a systematic error in the calculation of repolarization time. Though the best signal quality was achieved with the 7×7 filter, the additional improvement was only slightly better than that achieved with the 5×5 kernel, and comes at a significantly greater computational cost.

Table II.1: Error Distribution Statistics of AP Characteristics:
Values were computed following the application of three different sized Gaussian convolution kernels (3×3, 5×5, 7×7) without and with phase correction.

	Unfiltered	3×3 $\sigma = 0.631$	5×5 $\sigma = 1.179$	7×7 $\sigma = 1.475$
	Percent mean signed difference of the rate of depolarization			
Unshifted	0.06±3.80	5.85±2.30	12.88±3.93	18.43±4.88
Phase-shifted		1.55±1.70	0.78±1.11	0.63±0.98
	Percent mean absolute difference of the signal magnitude during repolarization			
Unshifted	4.00±0.53	1.11±0.23	0.65±0.15	0.57±0.14
Phase-shifted		1.06±0.23	0.61±0.13	0.49±0.11
	Percent signed difference of activation time			
Unshifted	0±2.00	0±0.20	0±0.35	0±0.47
Phase-shifted		0±0.13	0±0.11	0±0.11
	Percent signed difference of repolarization time			
Unshifted	0±0.36	-0.12±0.19	-0.24±0.27	-0.36±0.36
Phase-shifted		0±0.19	0±0.13	0±0.12

II.D.3 Discussion

The improvement in signal quality due to phase correction was not substantial until the range of phase shifts within the pixel neighborhood used for spatial averaging was equal to or greater than the sampling period. The range of phase shifts is influenced by many factors. As spatial resolution or conduction velocity increases, the range of neighborhood phase shifts decrease. However, camera capabilities and the area of tissue that is imaged limit spatial resolution. Increas-

ing temporal resolution or the size of the spatial filter will increase the range of phase shifts (greater number of time-sampling indices). Thus, as optical mapping studies are performed in mice, for example, the increase in conduction velocity and spatial resolution will be offset by the required increase in sampling frequency to resolve the action potentials properly, bolstering the utility of this algorithm.

II.E Efficient and Robust Data Processing

II.E.1 Data Masking

The optical signal from each pixel was checked for proper morphology. If a pixel recorded myocardial electrical activity, then the minimum digital number of the signal should be greater than 60 for 8-bit images (typical: 180 to 240), and have a range of digital numbers of more than 2 (typical: 10-15). For 12-bit images, these cutoff values are 960 and 3, respectively. Only those signals that achieve these minimum requirements and neighbor other acceptable signals were analyzed further. Excluded pixels were typically unusable due to curvature of the heart, saturation, or simply lying outside the bounds of the heart. This masking of the data set significantly improved temporal efficiency, as some data sets recorded valid signals at only 8,000+ pixels of a possible 16,128. Masking can also improve overall accuracy, especially in the measurement of field variables such as conduction velocity, as these measurements are based on differences between pixels and can be sensitive to spurious values.

II.E.2 Multiple Action Potential Signal Filtering and Analysis

The original algorithms required that single action potentials be parsed from the data set, then separately pre-processed, filtered, and analyzed. These routines were re-implemented to handle multiple action potential signals. The

basic process of phase-shift filtering, as previously described, [5] did not need to be altered, as these principles are independent of the signal. After filtering, the data set was automatically parsed by searching for action potential upstrokes and comparing/matching with electrocardiogram data, which had been analyzed for individual activations by looking for relatively large deflections (QRS waves), and comparing and matching to a user supplied pacing protocol. A graphical user interface was also developed that allows manual, but faster, parsing of complex data sets. After parsing, sections of data that contain a single optical action potential were analyzed for activation times, by searching for the maximum rate of rise of the action potential upstroke, and were analyzed for repolarization times at user defined levels of recovery from maximum amplitude. Conduction velocity vector fields were calculated from the reciprocal gradient of the fit to the local activation time field, as described by Bayly et al. [8]

II.E.3 Improved Accuracy and Robustness

Though the basis of the phase-shifting filtering algorithm was already in place, several details of implementation were improved. Proper accounting for filter scaling and transients was added. Algorithms to extract activation times and action potential durations from optical action potentials were made more robust to protect against spurious values due to the effects of signal noise and drift. Measurements of action potential duration were also vulnerable to error due to premature beats elicited during repolarization, which are frequently encountered during restitution studies. Figures II.2, II.3, and II.4 are examples of the improved robustness of these algorithms.

II.E.4 Improved Efficiency

Memory efficiency was improved, as previously, large data sets were passed intact down several recursed layers of sub-functions. Large variables are now passed by reference, and subsections of data are passed where appropriate.

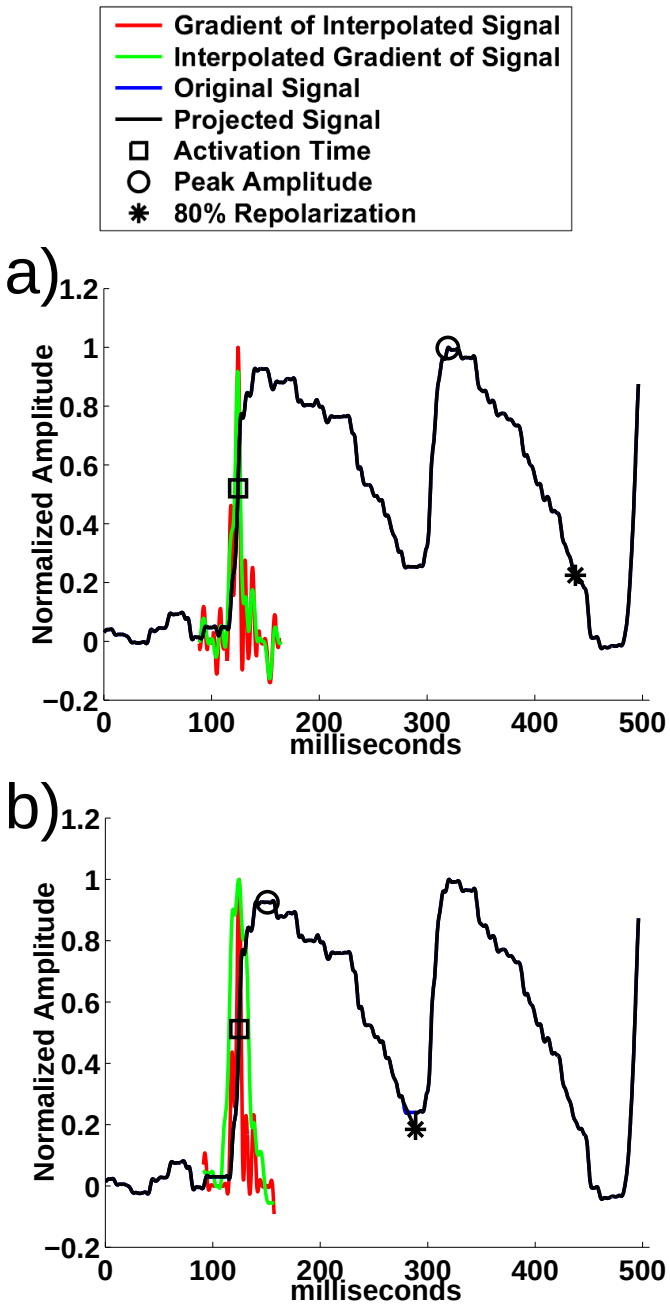

Figure II.2: (a) Example of original detection of optical action potential features in an S1 - S2 pacing protocol. (b) The same data with improved algorithms. S1 - S2 protocols cannot always be parsed, as short coupling intervals will elicit excitation while late-activated regions are still in the early repolarization stage.

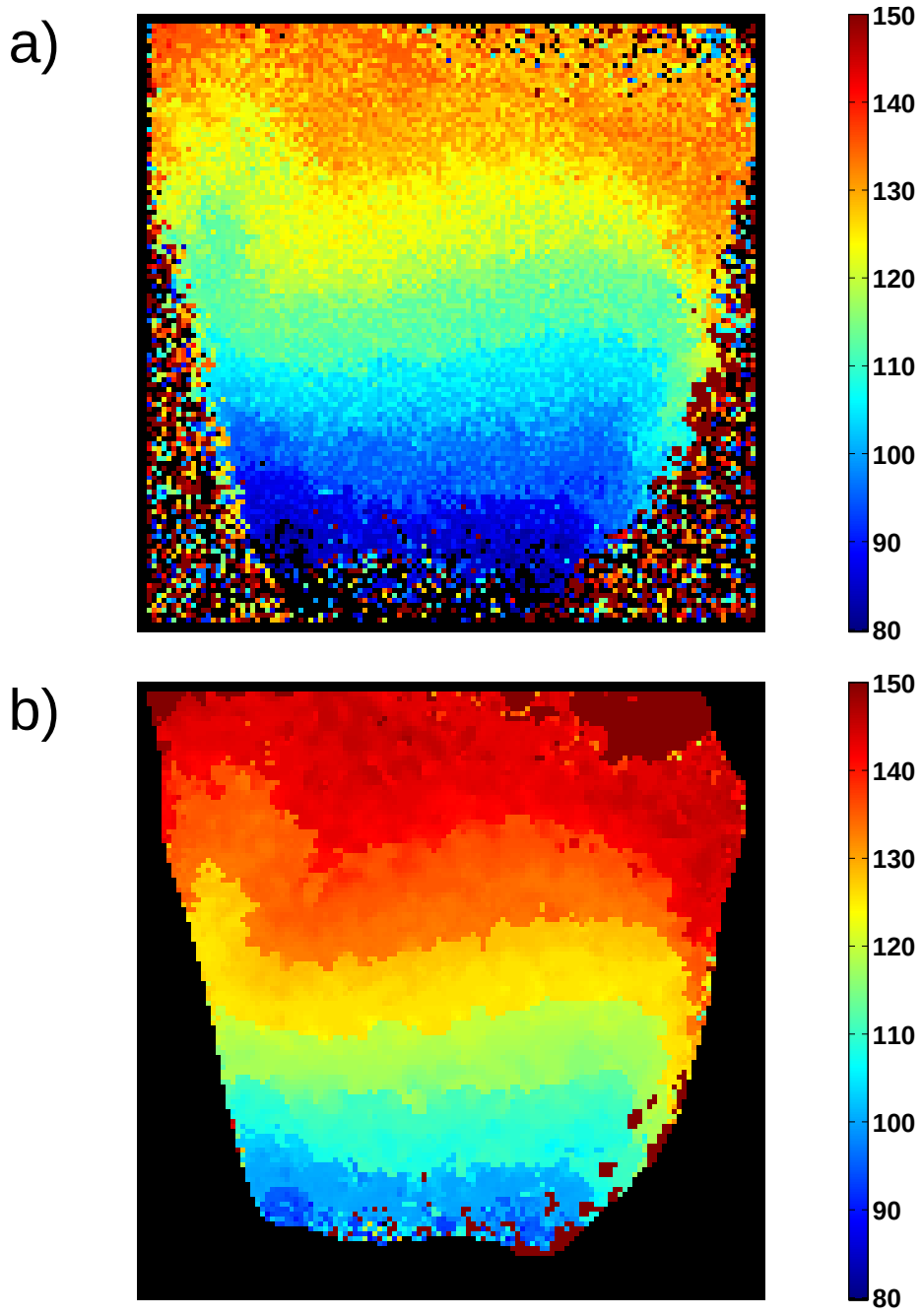

Figure II.3: (a) Example of activation map using original filtering and analysis algorithms in an S1 - S2 pacing protocol. (b) The same data with improved algorithms. Color bar indicates milliseconds.

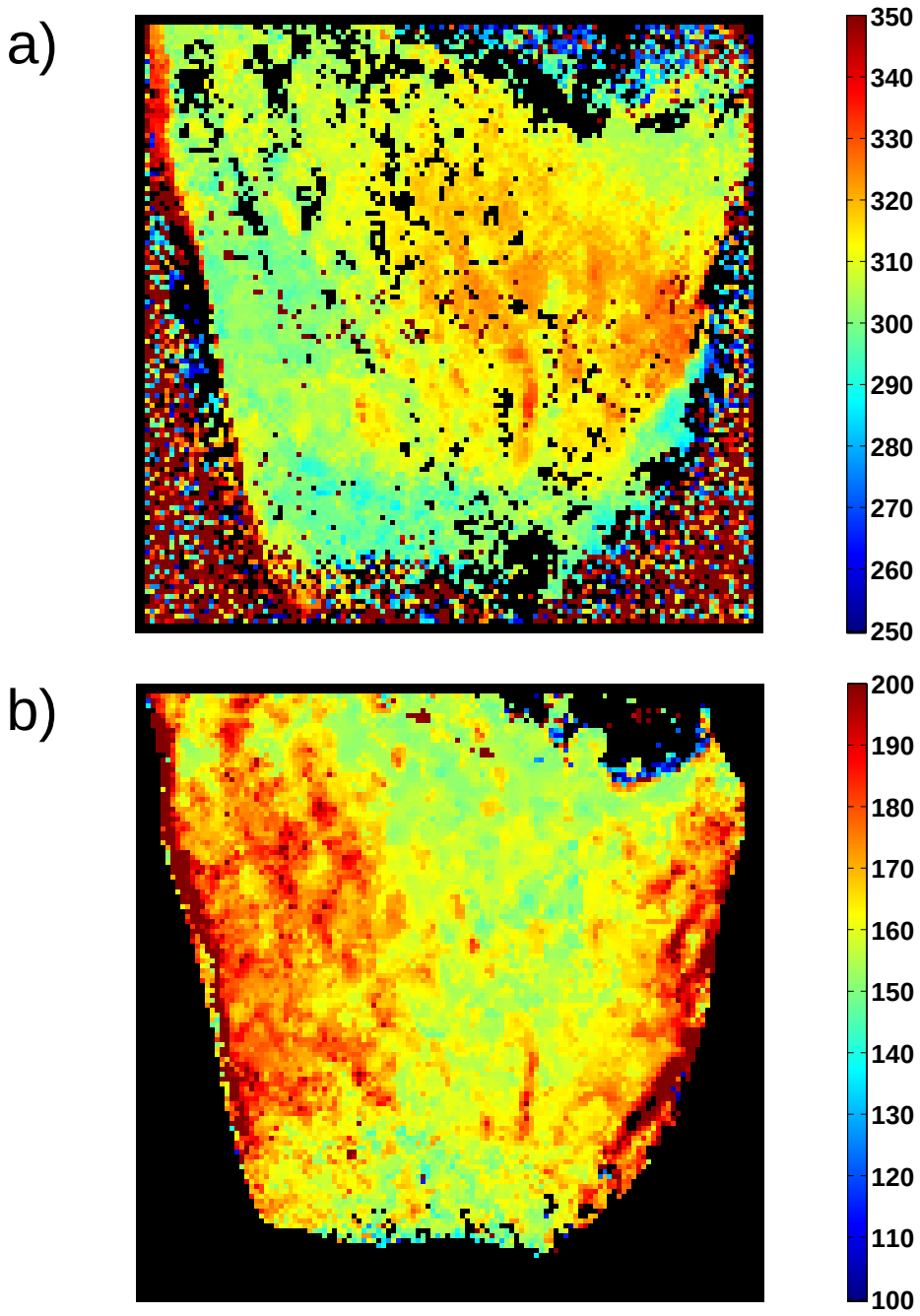

Figure II.4: (a) Example of APD_{80} map using original filtering and analysis algorithms in an S1 - S2 pacing protocol. (b) The same data with improved algorithms. Color bar indicates milliseconds.

Previously, each action potential to be analyzed was manually parsed from the data set, and the series of filtering algorithms were manually called. In addition to auto-parsing, several algorithms have been written to batch process concurrent data sets. Graphical user interfaces have been developed to assist where manual intervention is required, and to assist in visual analysis of complex data sets. These improvements in speed and efficiency allow the routine analysis of large data sets, where more than 50 runs of 2 second data, each including approximately 5 action potentials when pacing at a cycle length of 360 ms.

The text and figures of this chapter, in part, are a reprint of the material as it appears in: Sung D, Somayajula-Jagai J, Cosman P, Mills RW, McCulloch AD. Phase shifting prior to spatial filtering enhances optical recordings of cardiac action potential propagation. *Ann Biomed Eng.* 2001;29(10):854-861. The dissertation author was the primary researcher and author of the work presented here, and the co-authors listed in this publication directed and supervised the research that forms the basis for this chapter, or were primary researchers of material *not* presented here.

Appendix: Relevant MATLAB Code Table of Contents

```
% Phase-Shift Filtering and Utility Functions
%
% M-files used in:
%    Sung, D, et al.; Phase Shifting Prior to Spatial Filtering Enhances
%    Optical Recordings of Cardiac Action Potential Propagation; Annals
%    of Biomedical Engineering; 2001, v29 pp854-861
%
%    Contact: Andrew McCulloch, Ph.D.
%             Cardiac Mechanics Research Group
%             Dept. of Bioengineering
%             University of California San Diego
%             9500 Gilman Dr., La Jolla, CA 92093-0412
%             amcculloch@ucsd.edu
%
% Copyright (c) 2004 CMRG - UCSD Bioengineering
%    Any copy of these m-files must include this contents file
%    with this header unaltered.
%
%
%
%
% NOTE: Several of these functions (especially Batch Processing Scripts)
% assume that data is stored in files with the naming structure: r[run
% number]vars, with one variable per run.  Each file may contain several
% different variables with assumed (and if called in the appropriate
% order, already given) naming structure. See 'domanymultiAP' for more.
%
%
%-------------------------------------------------------------------------
%
% Loading and Saving
%   bmpstack        - Create an image stack from many sequentially named
%                       .BMP's
%   rhf             - Load an HPVEE (now LABVIEW) data file
%
%-------------------------------------------------------------------------
%
% Batch Processing Scripts (must be altered for use)
%   bmptomat        - Create .MAT variables from several runs stored in
%                       .BMP's
%   domanymultiAP   - Filter and analyze multiple runs of data
%   manrange        - Manual ranging of AP's
%
%   Specific Utility Functions:
%       runmanrange
%
%-------------------------------------------------------------------------
%
% Visualization
%   makemovie       - Creates a MATLAB movie from an image stack
```

```
51 %   showmap         - Displays maps of extracted AP features
52 %   viewAPinfo      - Allows one to scroll over image and see associated
53 %                       signals
54 %
55 %-------------------------------------------------------------------------
56 %
57 % AP Filtering and Parameter Extraction
58 %   APranges        - Determines approriate ranges for individual AP's
59 %                       from a multi-AP image stack
60 %   apfeaturesB     - Extracts activation anf repolarization features
61 %                       from AP
62 %   extpaceinfo     - Extracts pacing info from a pace artifact signal
63 %   extractmultiaps - 'apfeaturesB' over a map over all AP's
64 %   filtermultiaps  - Normalizes and filters an image stack
65 %   makegradvect    - Creates a vector used to approximate a gradient
66 %   makephaseap     - Forms the phase version of an AP signal
67 %   makesmthvect    - Creates a vector used to smooth a signal
68 %   normmultiaps    - Normalizes signals, creates information mask
69 %   phasefiltgen    - Sets up spatial and temporal filtering
70 %   timeshift       - Calculates time shift between two similar signals
71 %   unshift         - Time shifts a signal vector
72 %
73 %   Specific Utility Functions:
74 %       apmaps          - Working part of 'extractmultiaps'
75 %       initranges      - Initialzes the 'rngs' variable
76 %       rngmatch        - Matches data and image range sets
77 %
78 %-------------------------------------------------------------------------
79 %
80 % Restitution Analysis
81 %   restextract - Extract restitution information from several points
82 %
83 %   Specific Utility Functions:
84 %       restextract2        - The working part of restextract
85 %       restextract2_reapd  - The same, but with re-APD'ing
86 %       restcheck           - Shows data that gave a point on restitution
87 %                               curve
88 %       restcheckbutton     - Sets up 'restcheck' capability
89 %
90 %-------------------------------------------------------------------------
91 %
92 % General Utility Functions Used Various Places
93 %   Bobroipoly      - Select a ROI polygon, tracked in multiple axes
94 %   Bobgetline      - Select a line, tracked in multiple axes
95 %   drawline        - Draws lines with text on figure
96 %   errorbar_logx   - Use to draw error bars on log plots
97 %   expfitfunc      - Fit an exponential function to data
98 %   genincexp       - Generalized increasing exponential function
99 %   getpixel        - Get a pixel location from a map/image
100 %   looseroipoly    - Select a ROI freely, calls 'loosegetline'
101 %   medianap        - Median filter an AP (or any signal)
102 %   nicegrad        - Takes the gradient, 2nd order, and handles
```

```
103 %                         transients
104 %   nicesmooth      - Applies a smoothing vector and handles transients
105 %   outliers        - Useful for determining outliers of a data group
106 %   pointerfollow   - Tracks motion in one axis in another
107 %   rngcheck        - Checks validity of ranges
108 %   weightedlsqcurvefit - Adjusts 'lsqcurvefit' so that data can
109 %                           be weighted
110 %
```

References

[1] Tranquillo JV, et al. Genesis of the monophasic action potential: Role of interstitial resistance and boundary gradients. *Am J Physiol Heart Circ Physiol.* 2004;286(4):H1370-1381.

[2] Efimov IR, Nikolski VP, Salama G. Optical imaging of the heart. *Circ Res.* 2004;95(1):21-33.

[3] Loew LM, et al. A naphthyl analog of the aminostyryl pyridinium class of potentiometric membrane dyes shows consistent sensitivity in a variety of tissue, cell, and model membrane preparations. *J Membr Biol.* 1992;130(1):1-10.

[4] Knisley SB, et al. Ratiometry of transmembrane voltage-sensitive fluorescent dye emission in hearts. *Am J Physiol Heart Circ Physiol.* 2000;279(3):H1421-1433.

[5] Sung D, et al. Phase shifting prior to spatial filtering enhances optical recordings of cardiac action potential propagation. *Ann Biomed Eng.* 2001;29(10):854-861.

[6] Sung D, et al. Ventricular filling slows epicardial conduction and increases action potential duration in an optical mapping study of the isolated rabbit heart. *J Cardiovasc Electrophysiol.* 2003;14(7):739-749.

[7] Rogers JM, McCulloch AD. Nonuniform muscle fiber orientation causes spiral wave drift in a finite element model of cardiac action potential propagation. *J Cardiovasc Electrophysiol.* 1994;5(6):496-509.

[8] Bayly PV, et al. Estimation of conduction velocity vector fields from epicardial mapping data. *IEEE Trans Biomed Eng.* 1998;45(5):563-571.

Chapter III

Experimental Validation

III.A Abstract

Conduction slowing in response to ventricular volume loading was validated by excluding several potentially confounding factors. The effect of volume loading was still present despite improved oxygen delivery with a synthetic oxygen carrier, indicating that the effect is not a result of global ischemia. Measurement of regional tissue perfusion with microspheres indicated that loading uniformly decreases perfusion, suggesting that the effect of loading is not due to regional ischemia. Conduction slowing during loading was greater than that due to perfusate hypothermia resulting in equivalent epicardial surface temperatures, indicating that conduction did not slow due to a loading associated decrease in temperature. Because the optical mapping technique required the use of the voltage-sensitive dye, di-4-ANEPPS, and the excitation-contraction uncoupler, 2,3-butanedione monoxime, measurements with epicardial electrodes were performed without these reagents and indicated that incremental loading within a physiological range still led to incrementally longer activation times (slowed conduction).

III.B Introduction

Previously, it has been observed using the non-contact optical mapping technique that passive ventricular volume load slows apparent epicardial conduction and increases action potential duration at both early (20%) and late (80%) repolarization levels. [1] However, several potentially confounding factors must be accounted for:

1) Passive ventricular volume loading is applied by inflation of intraventricular balloon. This could increase total coronary resistance and reduce myocardial perfusion, which could potentially induce global ischemia, which would slow conduction. [2] Further, the effect of loading on activation times (from which conduction velocity is derived) appears to be greater at points distal to the pacing site, where conduction is primarily epicardial reactivation from the faster conducting endocardium, (a consequence of the differences in epi- and endo- fiber orientation between the pacing site and conduction sampling sites). [1] Thus, the latex balloon could be impinging on endocardial perfusion, while only moderately affecting total coronary inflow, and thus significantly slowing conduction by causing regional ischemia.

2) To minimize the phototoxic effects of the decomposition products of the voltage-sensitive dye, di-4-ANEPPS, the dye and excitation light are limited, resulting in a light limited fluorescent signal. In order to collect the maximal emitted light and to allow access for pacing and electrocardiogram electrodes, the isolated heart preparation is allowed to hang freely, such that the epicardial surface is exposed to room-temperature air. Consequently, the slight reduction in perfusion caused by passive inflation may decrease the epicardial surface temperature and result in slowed conduction. [3, 4]

3) Optical mapping of mechano-electric feedback in the Langendorff-perfused isolated rabbit heart was performed with di-4-ANEPPS, a fluorescent probe

used to visualize myocardial electrical activity, and 2,3-butanedione monoxime, an excitation-contraction uncoupler, used to inhibit motion artifact in acquired images. It is possible that exposing the myocardium to these agents results in loading associated changes in conduction velocity.

III.C Methods

III.C.1 Isolated Heart Preparation

All experiments were conducted using isolated Langendorff perfused rabbit heart preparations under animal use protocols reviewed and approved by the UCSD Animal Subjects Committee. 11 New Zealand white rabbits (2.5 - 3.0 kg) were sedated with a subcutaneous injection of ketamine (50 mg/kg) and xylazine (4 mg/kg) and anesthetized to a surgical plane with intravenous administration of sodium pentobarbital (30 mg/kg). A tracheotomy was performed to intubate and ventilate the animals with a mechanical respirator. Heparin (1,000 units/kg) was delivered intravenously. Following thoracotomy, the heart was arrested with a hyperkalemic cardioplegic solution (30 mM KCl) and rapidly excised.

The aorta was immediately cannulated, and the coronary arteries were perfused retrograde with a warm (35° - 37°C) oxygenated (95% O_2, 5% CO_2) modified Tyrodes solution: (130 mM NaCl, 4 mM KCl, 1.0 mM $CaCl_2$, 1.0 mM $MgCl_2$, 24 mM $NaHCO_3$, 1.2 mM NaH_2PO_4, 10.0 mM Dextrose). The left ventricle (LV) was vented with a small drain tube at the apex, and a latex balloon was inserted into the LV through an incision in the left atrium and secured at the mitral apparatus with a purse string suture. The balloon was connected to a fluid-filled pressure transducer as well as a servo-controlled volume infusion pump.

III.C.2 Optical Mapping Technique

The voltage-sensitive dye, di-4-ANEPPS, which was dissolved in DMSO and diluted to 10.4 μM with Tyrodes solution. A 10 mL bolus of this dye solution was injected into the perfusion line to stain the tissue. Additional injections of 5 ml of the dye solution were applied as needed. The electromechanical uncoupling agent 2,3-butanedione monoxime (BDM, 12.5 mM) was added to the perfusate to eliminate motion artifact. BDM was washed out immediately after data acquisition. The heart was paced at twice diastolic threshold and with a cycle length of 300 msec from the LV apical epicardium.

The hardware configuration for optical mapping has been described earlier. [5] Briefly, excitation light from a 300 Watt xenon arc lamp (Oriel Instruments, Stratford, CT) was passed through a dichroic mirror to filter out ultraviolet and infrared components and subsequently through a 516 $\pm$ 45 nm band-pass filter. The excitation light beam was then split with a bifurcating fiber optic bundle and directed as uniformly as possible onto the surface of the LV free wall. An electronic shutter limited excitation light exposure to a few seconds per run, thus minimizing the phototoxic and photobleaching effects of the dye. The emitted fluorescence was passed through a ¿ 610 nm high-pass filter and focused with a fast 50 mm lens (1:0.95, Navitar, Rochester, NY) onto an 8-bit CCD camera (Dalsa, Waterloo, Ontario model CA-D1-256). The optical images of the LV free wall (lateral view) were captured at a speed of 399 frames/second and a resolution of 128 $\times$ 126 pixels imaging an approximate 16-cm^2 area.

III.C.3 Optical Mapping Experimental Protocol

Following cannulation, the hearts were perfused with Tyrodes solution and allowed to actively contract. The initial volume (V_0) in the balloon was adjusted to an end diastolic pressure (EDP) of $\approx$0 mmHg, resulting in systolic pressures between 60 and 80 mmHg. The myocardium was mechanically preconditioned three times by infusing and withdrawing volume into the balloon at a

rate of 10 ml/min to a peak EDP of 30 mmHg. On the final preconditioning run, the volume at EDP = 30 mmHg was recorded, and the LV was loaded to this set volume (V_1) during the subsequent loading protocols.

From preliminary observations, we noted that the addition of BDM to the perfusate resulted in an increase in passive stiffness of the myocardium over a time course of approximately 20 minutes. However, within the first 5 minutes myocardial stiffness increased only slightly (4 to 6 mmHg at fixed LV volume), consequently, all experimental data were taken within 5 minutes after switching to the BDM-containing perfusate, with 1 minute given to allow motion to subside. Optical electrophysiological data were collected for 1 second from the 'initial unloaded' (V_0), 'loaded' (V_1), and 'final unloaded' (V_0) states. The LV balloon was infused or effused at 10 ml/min, and a 1 minute stabilization period was allowed after each state change. The perfusate was switched back to a BDM-free solution immediately following the protocol.

III.C.4 Conduction Velocity Analysis

Optical data were processed and phase-shift filtered as previously described. [5, 6] After filtering, activation times at each pixel were extracted as the time of the maximum rate of rise of the optical action potential upstroke. The apparent epicardial conduction velocity vector field was calculated from the reciprocal gradient of the activation time field as described by Bayly et al. [7]

III.C.5 The Effect of Increased Oxygen Delivery

A separate study of n = 3 hearts was studied to examine how increased oxygen delivery affected changes in apparent epicardial conduction velocity and action potential duration during mechanical loading. The perflubron emulsion oxygen carrier (*Oxygent*^{TM}, a gift from Alliance Pharmaceutical Corp., San Diego, CA) was mixed into the perfusate at 20% by volume, and this mixture was continuously agitated and oxygenated with 95% O_2, 5% CO_2. Because the oxygen carrier

obscured optical signals, an epicardial monophasic action potential (MAP) probe (EP Technologies, Sunnyvale, CA; 200 model) was used to record MAP's during loaded and unloaded states, before and after the addition of the oxygen carrier to the perfusate. All MAP recordings were taken at the posterior LV base during apical pacing. The LV was incrementally loaded to the volume, V_1, at which EDP was 30 mmHg. The preparation was unloaded and returned to sinus pacing for 30 seconds between successive applications of loads, and allowed to stand at each load state for 30 seconds before recordings were taken. Activation time was measured as the time from the pacing artifact to the maximum first derivative of the MAP phase 0, and APD_{90} was measured as 90% recovery from maximum of phase 2 to the median of phase 4.

III.C.6 Regional Perfusion

In a separate study of n = 2 hearts, fluorescent microspheres (Interactive Medical Technologies, Ltd., Irvine, CA) were used to determine how loading to an EDP of 30 mmHg affected myocardial perfusion distribution in the left ventricle. 250×10^3 microspheres, 15 μm in diameter, were injected into the perfusion line when the heart was unloaded and another bolus of microspheres labeled with a different fluophore was injected while the LV was loaded, both in the presence of BDM. In one heart of two, microspheres were injected while the preparation was perfused with a mixture of Tyrodes, BDM, and the synthetic oxygen carrier. A third set of microspheres was injected in this heart during normal Tyrodes and BDM perfusion as a reference. Total coronary inflow was measured using an in-line ultrasonic flow probe (Transonic Systems, Ithaca, NY; model 2N). The free wall of the left ventricle was removed and snap-frozen in embedding media using liquid nitrogen. The LV was cut into epi-, mid-, and endocardial pieces, weighed, and then analyzed for microsphere content by Interactive Medical Technologies, Ltd., Irvine, CA. Regional myocardial perfusion was calculated from the fraction of total injected microspheres found in each tissue piece and the total coronary

inflow.

III.C.7 The Effect of Loading on Epicardial Surface Temperature

In a separate study of n = 2 hearts, a thermocouple was used to record epicardial surface temperature before and during ventricular volume loading to 30 mmHg. In a follow-up study of n = 2 hearts, conduction velocity was assessed at 0 and 30 mmHg as a baseline, after which conduction velocity was repeatedly assessed as epicardial surface temperature decreased from nominal (34°C at a perfusate temperature of 37°C) to 33°C at 0.4°C/min by switching off the heated waterbath that warmed the perfusate. In a secondary follow-up study of n = 2 hearts, epicardial surface temperature was again monitored before and during loading, but the isolated heart preparation was modified such that the pulmonary artery was tied-off, and a small incision made in the artery just before it crosses-over the left atrium, so that warm saline that collected in the right ventricle constantly super-fused the epicardium of the left ventricle.

III.C.8 The Effect of BDM and di-4-ANEPPS

BDM was required in the perfusate to mechanically decouple the heart so that repolarization could be imaged without motion artifact. A separate study of n = 4 hearts was studied to examine the effects BDM may have had on apparent epicardial conduction velocity and action potential duration as a function of ventricular loading. Further, these studies were performed without di-4-ANEPPS. Bipolar electrograms were recorded while using the same pacing and loading protocols as above and a probe with an inter-electrode distance of 1 mm. Bipolar electrograms activation times and activation recovery intervals (ARI) were measured from electrograms as in Keevil. [8]

III.D Results

III.D.1 The Effect of Increased Oxygen Delivery

Including oxygen carrier in the perfusate caused an immediate and reversible increase in total coronary inflow of 10% - 15% in 3 of 3 preparations. Figure III.1a shows MAP activation times from one study as a function of infused volume using Tyrodes and BDM perfusates with and without the oxygen carrier. Activation time increased with increasing load during Tyrodes and BDM perfusion, and this effect was also seen when the oxygen carrier was included. The oxygen carrier also decreased activation time at all load levels. Figure III.1b shows MAP APD_{90} values from the same study. APD_{90} increased with loading when perfused with Tyrodes and BDM, which was also seen when the oxygen carrier was included in the perfusate. The inclusion of the oxygen carrier also increased APD_{90} at all load levels. These changes were observed in all three hearts.

III.D.2 Regional Perfusion

Regional myocardial perfusion in the loaded ventricle when the oxygen carrier was added to the perfusate was similar to that in the unloaded state without the oxygen carrier. Figure III.2 shows myocardial perfusion distribution with the oxygen carrier included in the perfusate. The oxygen carrier caused a 40% - 60% increase in regional perfusion in the left ventricular free wall, though total coronary inflow only increased a mean 10% - 15%. Ventricular loading caused a nearly uniform decrease in perfusion of about 30% throughout the LV free wall in both hearts; total flow was reduced by approximately 10% in both hearts.

III.D.3 The Effect of Loading on Epicardial Surface Temperature

Volume loading to 30 mmHg caused epicardial surface temperature to decrease $\sim$0.5° - 1.0°C. Figure III.3 shows that increased load caused conduction to slow 8%, while allowing epicardial temperature to drop by 1.0°C from nominal

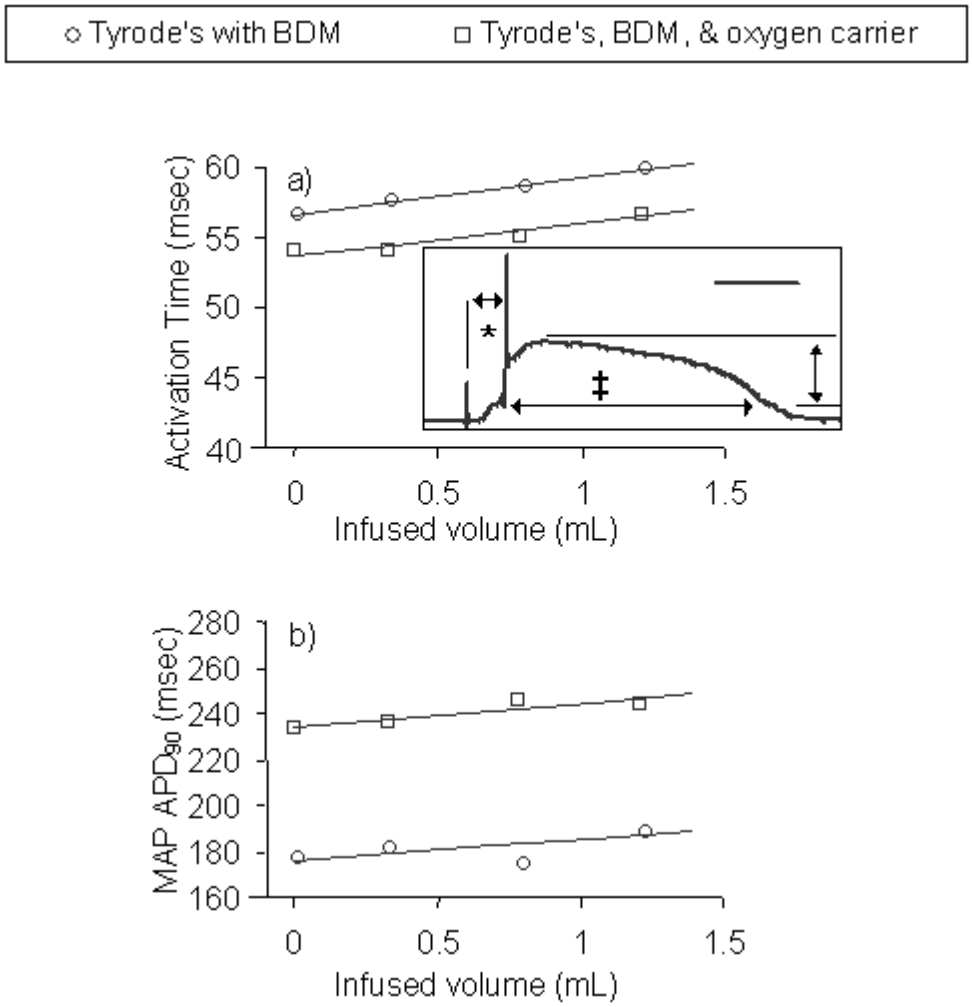

Figure III.1: The effect of increased oxygen delivery on (a) MAP activation time in heart R108 and (b) MAP APD_{90} in heart R108. The inset of (a) shows a typical MAP when the oxygen carrier was present, where $*$ indicates the activation time referenced from the pacing artifact, the vertical arrow indicates 90% recovery from peak value, and ‡ indicates APD_{90}. The calibration bar indicates 100 msec.

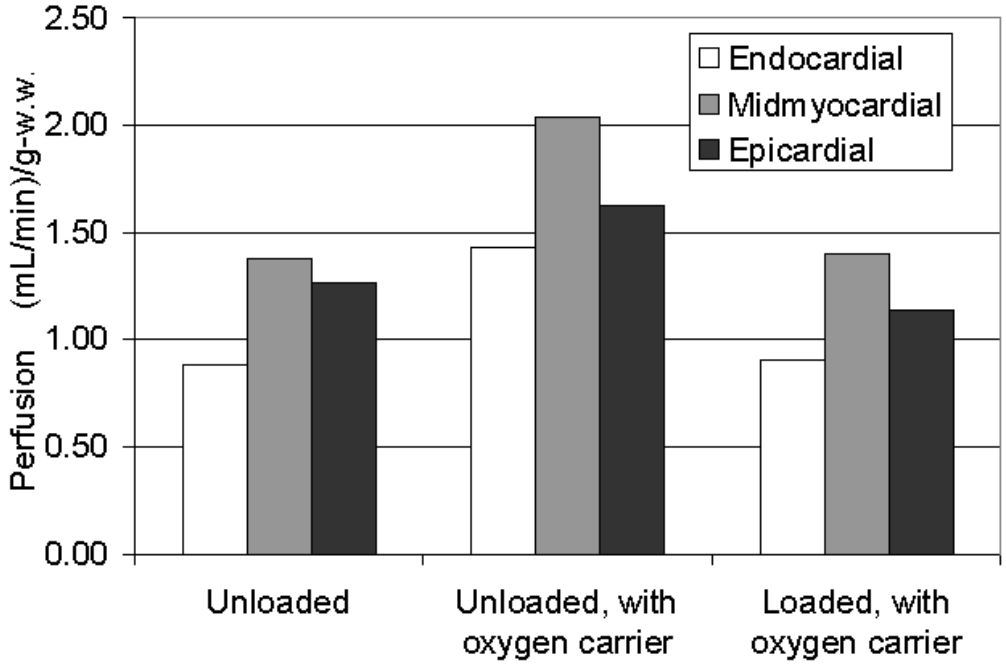

Figure III.2: Left ventricular free wall perfusion distribution as affected by the oxygen carrier and load.

caused conduction to slow 5%. Load decreased epicardial temperature, but this could be ameliorated by a slight modification of the preparation. In the final follow-up study with the modified preparation such that the left ventricular surface was constantly superfused with warm saline, the epicardial surface temperature change due to load was within the measurement error ($\pm$ 0.1°C).

III.D.4 The Effect of BDM and di-4-ANEPPS

Removing BDM from the perfusate reversibly decreased total perfusion to the preparation by a mean of 10%-20%. Figure III.4a shows bipolar electrogram activation times from one study as a function of infused volume using Tyrodes perfusate with and without BDM. Activation time increased with increasing load

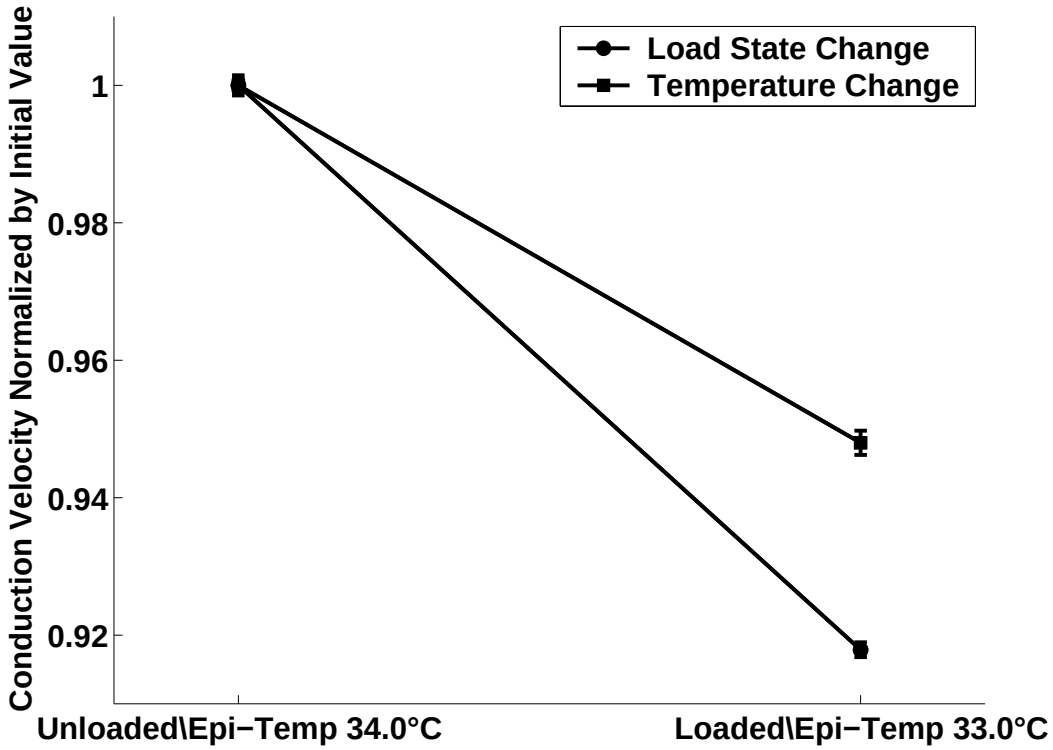

Figure III.3: The effect of 30 mmHg ventricular volume load vs. the effect of decreasing epicardial surface temperature by 1 degree.

during Tyrodes and BDM perfusion, and this effect was also seen when BDM was excluded. Removing BDM also decreased activation time at all load levels. These relationships were seen in all four hearts studied. Figure III.4b shows ARI's from another study versus infused volume. ARI increased with loading when perfused with Tyrodes and BDM, which was also seen when BDM was removed. The removal of BDM also increased ARI at all load levels. These relationships were observed in 3 of 4 hearts studied. In the fourth study, BDM containing perfusate had a relatively small positive correlation between load and ARI, while perfusate without BDM had a small negative correlation. These studies were performed in the absence of di-4-ANEPPS.

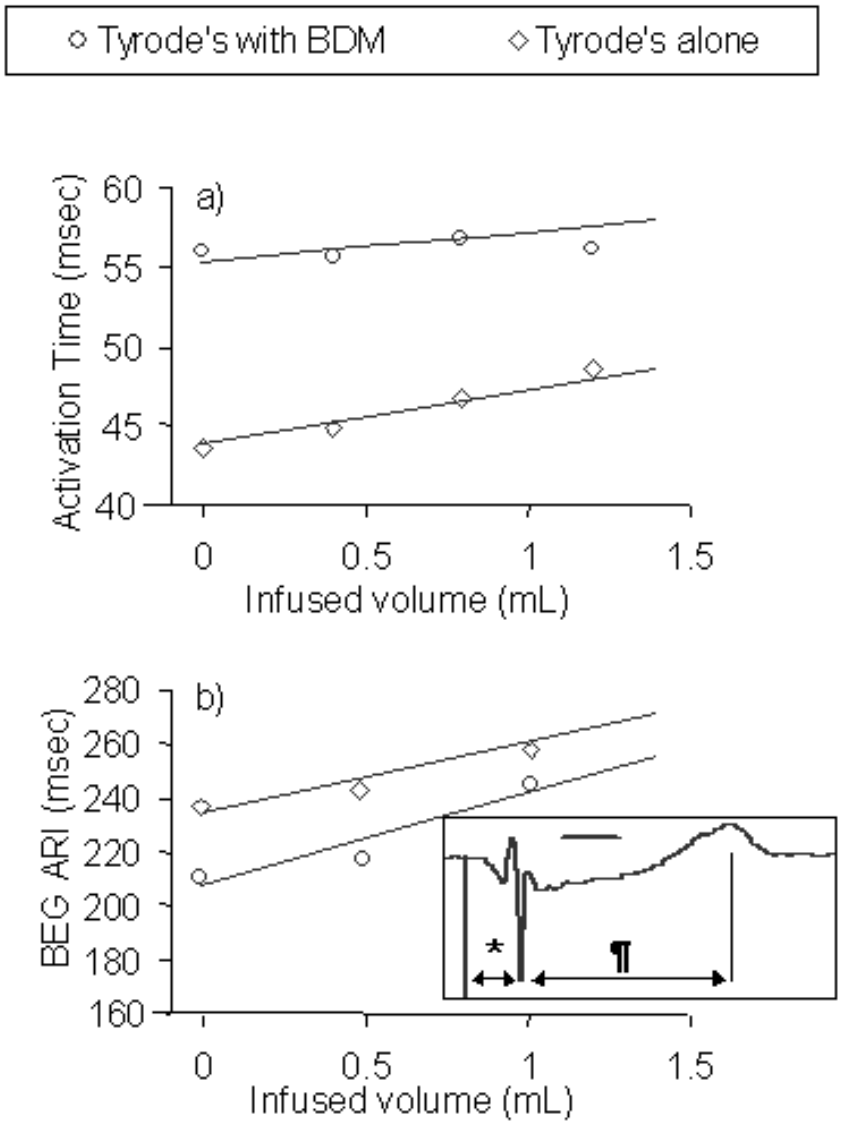

Figure III.4: The effect of removing BDM on (c) BEG activation time in heart R113 and (d) BEG activation recovery interval in heart R118. The inset of (d) shows a typical bipolar electrogram recording when BDM is not present, where $*$ indicates the activation time referenced from the pacing artifact, ¶ indicates the activation recovery interval. The calibration bar indicates 50 msec.

III.E Discussion

III.E.1 The Effect of Increased Oxygen Delivery

The observed decrease in CV in the loaded state could also be consistent with the effects of general ischemia. However, perfusion remained adequate despite a decrease in coronary inflow during loading. Edlund et al. [9] concluded that cardiac perfusion with saline that has been oxygenated at atmospheric pressure with a 5% CO_2, 95% O_2 mixture was sufficient, with low lactate production and submaximal coronary flow and fractional oxygen extraction. Moreover, Murashita et al. [10] concluded that a more metabolically demanding preparation, a working isolated rabbit heart, was adequately perfused with a bicarbonate buffer. In addition, BDM increased O_2 supply from baseline by inhibiting the increased resistance to coronary flow during contraction, and also reduced metabolic demand. Furthermore, the decrease in CV was still seen during increased oxygen delivery by the oxygen carrier.

Increased oxygen supply did not change observations or conclusions. Apparent conduction velocity, as inferred from the increase in activation time from the pacing to measuring electrodes, still decreased with the amount of applied load even when well oxygenated by the oxygen carrier. Moreover, supply-ischemia would tend to decrease APD, whereas an increase in APD_{90} was observed at all distances from pacing site. APD_{30} exhibited the same correlations, though the increase in magnitude was not as great as APD_{90} (not shown). In two hyperperfused preparations, perfusion pressure head was matched to the loading pressure (30 mmHg) and was applied just before recording to minimize edema. The same conduction velocity and APD trends were observed (not shown) as in the oxygen carrier studies.

These electrode studies indicate that load-induced supply-ischemia did not cause the decrease in apparent conduction velocity or increase in APD_{90} during optical mapping studies. As previously seen in optical mapping studies, [1] these

electrode studies also showed at least partial recovery of activation times and APD with unloading (not shown). The load dependent nature of these measurements further indicates that these observations cannot be mainly attributed to recovery from an ischemic episode.

III.E.2 Regional Perfusion

In the optical mapping studies, the decrease in apparent conduction velocity is greater distal from the pacing site, after the induced AP wavefront has propagated transmurally. This observation is not explained by subendocardial supply ischemia due to balloon loading. Microsphere measurements showed that perfusion was reduced nearly uniformly throughout the wall. Actual myocardial perfusion would be greater than reported due to microsphere loss, though loss should be consistent between microsphere sets. However, measured values when loaded were still greater than 0.75 mL/min/g-w.w.

III.E.3 The Effect of Loading on Epicardial Surface Temperature

Because volume loading caused a slight decrease in myocardial perfusion, and because the heart is exposed to room temperature air to optimize the collection of fluorescent light for the optical mapping technique, epicardial surface temperature decreased with loading. However, decreasing epicardial surface temperature to the lowest levels measured during ventricular loading slowed conduction less than ventricular loading. Further, the effect of loading on conduction is also observed distal to the pacing site, where conduction is primarily epicardial reactivation from the faster conducting endocardium (a consequence of the differences in epi- and endo- fiber orientation between the pacing site and conduction sampling sites), [1] where temperature would be minimally affected by loading. Finally, the modified isolated heart preparation had minimal decreases in epicardial surface temperature, and volume loading slowed conduction in subsequent studies using this preparation (see Chapter IV). These results show that the effect of loading acts independently

of a decrease in epicardial temperature.

III.E.4 The Effect of BDM and di-4-ANEPPS

To acquire the optical images of myocardial conduction, it was necessary to use the voltage-sensitive dye, di-4-ANEPPS. To prevent motion artifact in the optical measurements, it was necessary to add the electromechanical uncoupling agent BDM to the perfusate just prior to recording. Removal of BDM decreased activation time, consistent with previous reports that BDM slows conduction. [11, 12] However, the load-dependent increase of activation times observed with optical mapping was also seen using electrode recordings when neither di-4-ANEPPS nor BDM was present. These studies further show that neither agent had a significant impact on the trends observed or conclusions reached from the optical studies.

The effect of including BDM in the perfusate on APD is consistent with previous reports. [11, 13, 14] The increase in APD with load was seen when the preparation was perfused with saline and BDM, or when perfused with the saline/BDM/oxygen carrier mixture, but only usually seen when perfused with normal saline. This discrepancy in APD when normo-saline perfused may be due to ischemia from a combination of load-induced decrease in supply and increased demand, as compared to when mechanically decoupled. Additionally, ARI load correlation varied greatly in slope between interventions and preparations, and was highly dependent on specific protocol. Conversely, activation time trends were reasonably consistent between interventions, preparations, and differing protocols.

III.F Conclusions

These studies indicate that conduction slowing during ventricular volume loading is not a consequence of global or regional ischemia, nor due to a load associated decrease in epicardial surface temperature. These studies also in-

dicate that conduction slowing during volume loading still occurs in the absence of di-4-ANEPPS and 2,3-butanedione monoxime, which were necessary for the optical mapping technique. Further, these studies show that conduction slowing and action potential lengthening are correlated with the degree of loading within a physiological range, as incremental increases in load incrementally affect conduction and APD. These studies also led to an improved isolated heart preparation, wherein epicardial surface temperature is less impacted by loading.

III.G Acknowledgement

We acknowledge Michelle Mazzoni, Ph.D., of Alliance Pharmaceutical Corp., San Diego, CA, which made the gift of the oxygen carrier, $Oxygent^{TM}$.

The text and figures of this chapter, in part, are a reprint of the material as it appears in: Sung D, Mills RW, Schettler J, Narayan SM, Omens JH, McCulloch AD. Ventricular filling slows epicardial conduction and increases action potential duration in an optical mapping study of the isolated rabbit heart. *J Cardiovasc Electrophysiol.* 2003;14(7):739-749. The dissertation author was the primary researcher and author of the work presented here, and the co-authors listed in this publication directed and supervised the research that forms the basis for this chapter, or were primary researchers of material *not* presented here.

References

[1] Sung D, et al. Ventricular filling slows epicardial conduction and increases action potential duration in an optical mapping study of the isolated rabbit heart. *J Cardiovasc Electrophysiol*. 2003;14(7):739-749.

[2] Kleber AG, Riegger CB, Janse MJ. Electrical uncoupling and increase of extracellular resistance after induction of ischemia in isolated, arterially perfused rabbit papillary muscle. *Circ Res*. 1987;61(2):271-279.

[3] Kohlhardt M. Different temperature sensitivity of cardiac na+ channels in cell-attached and cell-free conditions. *Am J Physiol*. 1990;259(4 Pt 1):C599-604.

[4] Nygren A, et al. Voltage-sensitive dye mapping in langendorff-perfused rat hearts. *Am J Physiol Heart Circ Physiol*. 2003;284(3):H892-902.

[5] Sung D, Omens JH, McCulloch AD. Model-based analysis of optically mapped epicardial activation patterns and conduction velocity. *Ann Biomed Eng*. 2000;28(9):1085-1092.

[6] Sung D, et al. Phase shifting prior to spatial filtering enhances optical recordings of cardiac action potential propagation. *Ann Biomed Eng*. 2001;29(10):854-861.

[7] Bayly PV, et al. Estimation of conduction velocity vector fields from epicardial mapping data. *IEEE Trans Biomed Eng*. 1998;45(5):563-571.

[8] Keevil VL, et al. The effect of heptanol on the electrical and contractile function of the isolated, perfused rabbit heart. *Pflugers Arch*. 2000;440(2):275-282.

[9] Edlund A, Wennmalm A. Oxygen consumption in rabbit langendorff hearts perfused with a saline medium. *Acta Physiol Scand*. 1981;113(1):117-122.

[10] Murashita T, Kempsford RD, Hearse DJ. Oxygen supply and oxygen demand in the isolated working rabbit heart perfused with asanguineous crystalloid solution. *Cardiovasc Res*. 1991;25(3):198-206.

[11] Liu Y, et al. Effects of diacetyl monoxime on the electrical properties of sheep and guinea pig ventricular muscle. *Cardiovasc Res*. 1993;27(11):1991-1997.

[12] Sada H, Sada S, Sperelakis N. Effects of diacetyl monoxime (dam) on slow and fast action potentials of young and old embryonic chick hearts and rabbit hearts. *Eur J Pharmacol*. 1985;112(2):145-152.

[13] Banville I, Gray RA. Effect of action potential duration and conduction velocity restitution and their spatial dispersion on alternans and the stability of arrhythmias. *J Cardiovasc Electrophysiol*. 2002;13(11):1141-1149.

[14] Biermann M, et al. Differential effects of cytochalasin d and 2,3 butanedione monoxime on isometric twitch force and transmembrane action potential in isolated ventricular muscle: Implications for optical measurements of cardiac repolarization. *J Cardiovasc Electrophysiol*. 1998;9(12):1348-1357.

Chapter IV

Mechanisms of Conduction Slowing During Myocardial Stretch by Ventricular Volume Loading

IV.A Abstract

Introduction: Passive ventricular loading by volume inflation reversibly slows electrical conduction, but the mechanism behind this slowing remains unclear. The objective of these studies was to investigate the contributions of stretch-activated channels, depressed membrane excitability, increased intercellular resistance, and increased effective membrane capacitance during volume loading as the mechanism behind conduction slowing.

Methods and Results: Apparent conduction velocity was assessed using optical mapping in epicardially-paced, isolated perfused rabbit hearts at left ventricular end diastolic pressures of 0 and 30 mmHg. Inclusion of 50 μM gadolinium^{3+}, a stretch-activated channel blocker, in the perfusate attenuated the reversible increase in action potential duration during volume loading, but did not

alter the reversible slowing of conduction. Volume loading reduced conduction despite changes in membrane excitability caused by varying perfusate potassium concentrations from 1.5 - 8 mM.

Effective cross-fiber space and time constants, assessed by optical mapping of the tissue response to a cathodal-break point stimulus, increased significantly by 36 ± 8% (p = .02) and 64 ± 14% (p = .02), respectively.

Conclusions: Slowing of apparent epicardial conduction during myocardial stretch by ventricular volume loading is not significantly attributable to stretch-activated channels or depressed membrane excitability. Increased effective space and time constants indicate that volume loading may reduce intercellular resistance and increase effective membrane capacitance, resulting in a net slowing of conduction due to the greater sensitivity of conduction velocity to a change in capacitance.

IV.B Introduction

Several studies have linked volume overload or increased myocardial wall stretch with atrial and ventricular arrhythmias, [1] and reentrant arrhythmias are the predominant phenotype underlying those disturbances associated with mechanical dysfunction. [2] A reentrant circuit requires excitable tissue ahead of the activation wavefront (an 'excitable gap'), and thus is promoted and sustained by reduced refractoriness and slowed conduction. We have previously observed in isolated rabbit heart that passive ventricular loading by volume inflation slows conduction. [3] Other effects of mechanical stimuli on electrophysiology (broadly termed 'mechano-electric feedback') are frequently associated with the activation of stretch-activated channels. [4]

Conduction velocity (CV) is influenced by membrane excitability, as a faster phase 0 of the action potential more quickly creates the electrochemical gra-

dient that drives ionic diffusion along the membrane. The associated voltage-gated fast sodium conductances are regulated not only by ligand gating and autonomic stimulation, [5] but also by resting membrane potential. As resting potential depolarizes towards threshold, less charge is needed to achieve threshold, yet more sodium channels are trapped in the inactivated state, [6] resulting in a biphasic relationship between conduction speed and resting potential. [7] Myocardial stretch has been associated with a slight depolarization of resting membrane potential. [8]

Passive conduction speed is influenced by resistive and capacitive forces. [9] Although total mypolasmic resistance along a cell length is the primary resistance to longitudinal conduction, [10] gap junctions, which co-localize with several cellular structural elements, [11] further modulate longitudinal resistance to conduction, [7] yet, these recurring resistances reduce the downstream electrical load on the depolarizing wavefront. [12] Similarly, membrane capacitive load, which is governed by the membrane surface to cellular volume ratio, [9] can influence conduction speed as greater membrane capacitance requires more time for an upstream cell to charge its neighbor from resting potential to threshold, thereby slowing conduction.

The objective of these studies was to investigate the contributions of stretch-activated channels, membrane excitability depression, increased intercellular resistance, and increased membrane capacitance to conduction slowing during myocardial stretch by ventricular volume loading in isolated rabbit hearts. We conclude that stretch-activated channels do not significantly contribute to conduction slowing during volume loading, that volume loading does not significantly affect membrane excitability, that intercellular resistance is actually decreased by volume loading, and that conduction slowing during volume loading is predominantly a result of increased effective membrane capacitance.

IV.C Methods

IV.C.1 Isolated Heart Preparation and Experimental Protocol

All studies were performed using isolated Langendorff-perfused rabbit heart preparations as previously described [3] under animal use protocols approved by the UCSD Institutional Animal Care and Use Committee. Briefly, the heart was isolated and retrogradely perfused with warmed (35° - 37°C) and oxygenated (95% O_2, 5% CO_2) modified Tyrode's solution composed of: 130 mM NaCl, 4.5 mM KCl, 1.3 mM $CaCl_2$, 1.1 mM $MgCl_2$, 25 mM $NaHCO_3$, 1.2 mM NaH_2PO_4, 10.0 mM dextrose. Surface ECG and total coronary inflow were continuously monitored. The heart was apically paced at twice diastolic threshold at a cycle length of 360 ms. The left ventricle could be passively volume loaded to an end-diastolic pressure of 30 mmHg by inflating an intraventricular latex balloon connected to a pressure transducer, with 1-minute stabilization periods allowed between load state changes. Optical mapping data were taken for triplicate 2-second runs in the 'initial unloaded' (0 mmHg), 'loaded' (30 mmHg), and 'final unloaded' (0 mmHg) states.

IV.C.2 Optical Mapping

Optical mapping was performed as previously described. [3] Briefly, after staining with a 10 mL bolus of the voltage-sensitive dye, di-4-ANEPPS (10.4 μM), the dye was excited at 516 $\pm$ 45 nm from a 300 Watt xenon arc lamp. Epifluorescence was passed through a $>$ 610 nm filter and focused with a high numerical aperture lens (f/0.95, Navitar, Rochester, NY) onto an 8-bit CCD camera (Dalsa, Waterloo, Ontario model CA-D1-256) imaging an approximate 9-cm^2 area at 399 frames/second and a resolution of 128 $\times$ 126 pixels. Additional 5 mL dye injections were given as needed to maintain acquired fluorescent signal intensity. The electromechanical uncoupling agent 2,3-butanedione monoxime (BDM, 12.5 mM) was added to a secondary perfusate reservoir, which was used to perfuse the heart

during data acquisition, and was washed out immediately after data acquisition.

IV.C.3 Conduction Velocity Analysis

Optical data were processed and phase-shift filtered as previously described. [13, 14] After filtering, activation times at each pixel were extracted as the time of the maximum rate of rise of the optical action potential upstroke. The apparent epicardial conduction velocity vector field was calculated from the reciprocal gradient of the activation time field as described by Bayly et al. [15]

Conduction velocity is reported as mean magnitude from 4 consecutive action potentials and in the region near (1 - 5 mm) the stimulating electrode, which is composed primarily of epicardial cross-fiber conduction. [3] Assessment of mean CV was replicated in triplicate for each load state. Mean conduction velocities were then normalized by the mean initial unloaded value of the specific unload/load/unload series, so that comparisons of the effect of volume loading could be made at different time points within the same study and between individual preparations.

IV.C.4 Stretch-Activated Channels

Conduction velocity was measured in n = 4 hearts before and after 50 μM gadolinium^{3+} (Gd^{3+}), a non-specific blocker of stretch-activated channels (SACs), was added to the perfusates. Since Gd^{3+} precipitates out of carbonate/phosphate buffered saline, the perfusate was modified to a HEPES buffered solution: 140 mM NaCl, 4.5 mM KCl, 1.3 mM $CaCl_2$, 1.3 mM $MgCl_2$, 10 mM HEPES, 10.0 mM dextrose, titrated to pH of 7.4 and oxygenated with pure O_2. As a positive control of the effect of Gd^{3+}, action potential duration at the 30% and 60% repolarization levels (APD_{30} and APD_{60}) were concurrently measured by taking the difference between repolarization time at 30% or 60% recovery from peak value and activation time.

IV.C.5 Membrane Excitability

Conduction velocity was measured in n = 5 hearts as a function of potassium concentration to manipulate membrane excitability. [6, 7] The relationship between conduction velocity and perfusate potassium concentrations was evaluated at: 1.5, 2, 2.5, 3.5, 4.5 (normokalemic), 5.5, 6.5, and 8 mM.

IV.C.6 Effective Space and Time Constants

The effect of volume loading on the effective space and time constants was assessed in n = 4 hearts using similar methods to those of Poelzing et al., [16] in conjunction with assessment of conduction velocity. Because measured conduction velocities primarily reflected cross-fiber conduction, this study focused on the effective space and time constants in the cross-fiber direction. The magnification of the optical mapping system was increased to reduce the field-of-view to an approximate 2.25-cm^2, centered about a 125-micron-diameter Teflon-coated platinum wire contacting the mid-lateral LV freewall. After steady-state pacing from the apical electrode (100 paced beats), a 1 mA ($\sim$2$\times$ threshold) cathodal stimulus was delivered for 250 ms, with onset during phase 2 of the local action potential, resulting in a cathodal-break stimulus during phase 4. Optical signals were *not* temporally or phase-shift filtered, so that the tissue response to the stimulus was not artifactually propagated in space or time. Signals were normalized by baseline action potential amplitude so that the tissue stimulus response could be compared across space. The common mode signal (mean signal distal from the stimulus site) was subtracted from every pixel, leaving only the transmembrane voltage response to the stimulus.[Figure IV.1a-b] The steady-state stimulus response field[Figure IV.1c] (mean of the last $\sim$75 ms of stimulus) was fit to the steady-state approximate analytical solution to the bidomain equations. [17] These equations were modified by multiplying all terms by the dimensionless radius (coordinates normalized by the transverse and longitudinal space constants), as this better reflects the temporal and spatial averaging inherent in the optical mapping

technique. [16] The resulting equation when the coordinate system is rotated such that z is aligned with the local epicardial fiber direction, and x with the cross-fiber is:

$$\mathrm{M}_1 \left(\mathrm{e}^{-R} - \mathrm{M}_8 \left\{ \mathrm{e}^{-R} + \left[\frac{3}{\mathrm{R}^2} - \mathrm{e}^{-R} \left(1 + \frac{3}{\mathrm{R}} + \frac{3}{\mathrm{R}^2} \right) \right] \frac{3\cos^2(\Theta) - 1}{2} \right\} \right) \qquad \text{(IV.1)}$$

where

$$\mathrm{R} = \left[\left(\frac{\mathrm{x}}{\lambda_T} \right)^2 + \left(\frac{\mathrm{z}}{\lambda_L} \right)^2 \right]^{\frac{1}{2}} \qquad \text{and} \qquad \Theta = \tan^{-1} \left(\frac{\left(\frac{\mathrm{x}}{\lambda_T} \right)}{\left(\frac{\mathrm{z}}{\lambda_L} \right)} \right)$$

where Φ_m is the transmembrane potential, and where M_1 and M_8 are scaling parameters taken from the amplitude of the response at the center and nominal ratios of intracellular and extracellular conductivities, [17, 18] while the free parameters are the transverse and longitudinal space constants (λ_T and λ_L).

Mean strain induced by volume loading was used to correct loaded values of the effective space constant, such that all reported values are in terms of unloaded length (a constant material description; uncorrected effective space constant values are $\sim$1.05$\times$ larger). The transient response of epifluorescence to the stimulus was fit to a mono-exponential at all pixels near the stimulus site and in the cross-fiber direction. The mean exponential value was used as the effective time constant of the local tissue. Measurement of effective space and time constants was replicated in triplicate for each load state. Mean effective space and time constants were also normalized by the series mean initial unloaded values.

IV.C.7 Carbenoxolone

The effect of volume loading on conduction velocity and effective space and time constants was assessed in n = 3 hearts using perfusates without and with 50 μM carbenoxolone, a selective gap junction uncoupler. [19]

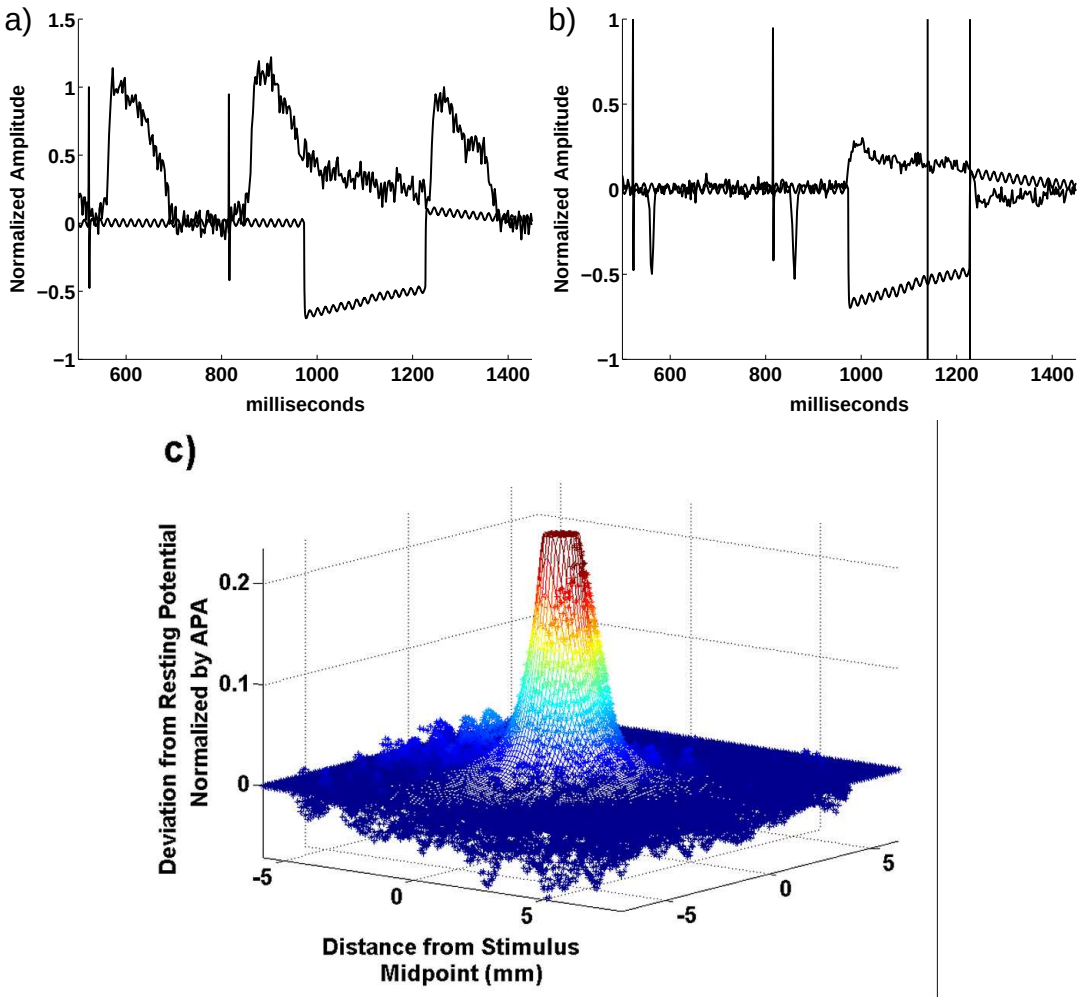

Figure IV.1: (a) Example signal showing transmembrane voltage response to cathodal-break stimulus. (b) The same signal after common mode rejection, and indicating the steady-state region. (c) Representative steady-state stimulus response and bidomain model fit.

IV.C.8 Statistics

All values are expressed as mean ± standard error of the mean. Conduction velocity and effective space and time constants were analyzed using repeated measures analysis of variance with load state and use of pharmacological agents as multiple within-factors where appropriate, and a post hoc Scheffe's F-test was used to differentiate load states when appropriate. Power is calculated as described by Cohen. [20]

IV.C.9 Multicellular Fiber Model Conduction Analysis

A model of conduction along a multicellular fiber was created as described by Shaw and Rudy, [21] with 3 discretizations per cell, and with the Saucerman et al. [22] implementation of the Puglisi-Bers rabbit ventricular myocyte ionic model, [23] an extension of the Luo-Rudy model. [24] The 70-cell fiber was stimulated at the first cell, and conduction velocity was calculated as the distance covered divided by the difference in activation times (calculated from the maximum derivative of the upstroke) between cell numbers 20 to 50. Effective intercellular resistance was increased to 250 Ω-cm so that baseline conduction velocity was slower than the nominal fiber direction conduction speed and similar to measured values of approximately 35 cm/s, as measured values reflect a large contribution of cross-fiber conduction. Conduction velocity was again calculated after increasing membrane capacitance 64%, the measured mean increase in effective time constant during volume loading, and again after decreasing intercellular resistance 45%, as implied by the measured mean increase in effective space constant (see below).

IV.D Results

IV.D.1 Stretch-Activated Channels

Inclusion of 50 μM Gadolinium^{3+} in the perfusate attenuated the increase in APD_{30} and APD_{60} during volume loading and prevented recovery to unloaded values, but Gd^{3+} did not significantly alter the reversible conduction slowing during volume loading. Mean initial unloaded APD_{30} was 103 ± 3 ms, increased 19 ± 3% ($p = .001$) during volume loading and recovered to 104 ± 2% of the initial value after load was removed. With Gd^{3+} present, mean initial unloaded APD_{30} was 105 ± 7 ms, but increased only 6 ± 7% during volume loading, and continued to increase to 113 ± 8% of the initial value after load was removed. This interaction of Gd^{3+} with the effect of loading on APD_{30} was significant ($p < .05$). The attenuation of the increase in APD_{60} during volume loading in the presence of Gd^{3+} was less pronounced, but the recovery of APD_{60} when loading was removed was still inhibited, and this interaction effect of Gd^{3+} was significant as well ($p < .01$). Figure IV.2 shows that mean initial unloaded CV was 30.8 ± 4.7 cm/s, decreased 12 ± 3% ($p = .01$) during volume loading and recovered to 95 ± 1% of the initial value. With Gd^{3+} present, all conduction values were similar: mean initial unloaded CV was 29.9 ± 4.8 cm/s, decreased 15 ± 7% during volume loading, and recovered to within 94 ± 2% of the initial value. The interaction effect on CV was not significant, while this study could detect a minimum 40% interaction effect (a 40% attenuation of slowing during loading due to the presence of Gd^{3+}) with a power of .8 or greater.

IV.D.2 Membrane Excitability

Varying perfusate potassium concentration did not significantly alter the effect of volume loading on conduction velocity. Figure IV.3 shows that in the range of concentrations studied, altering perfusate potassium concentration from normokalemic slowed conduction. This relationship was similar before, during, and

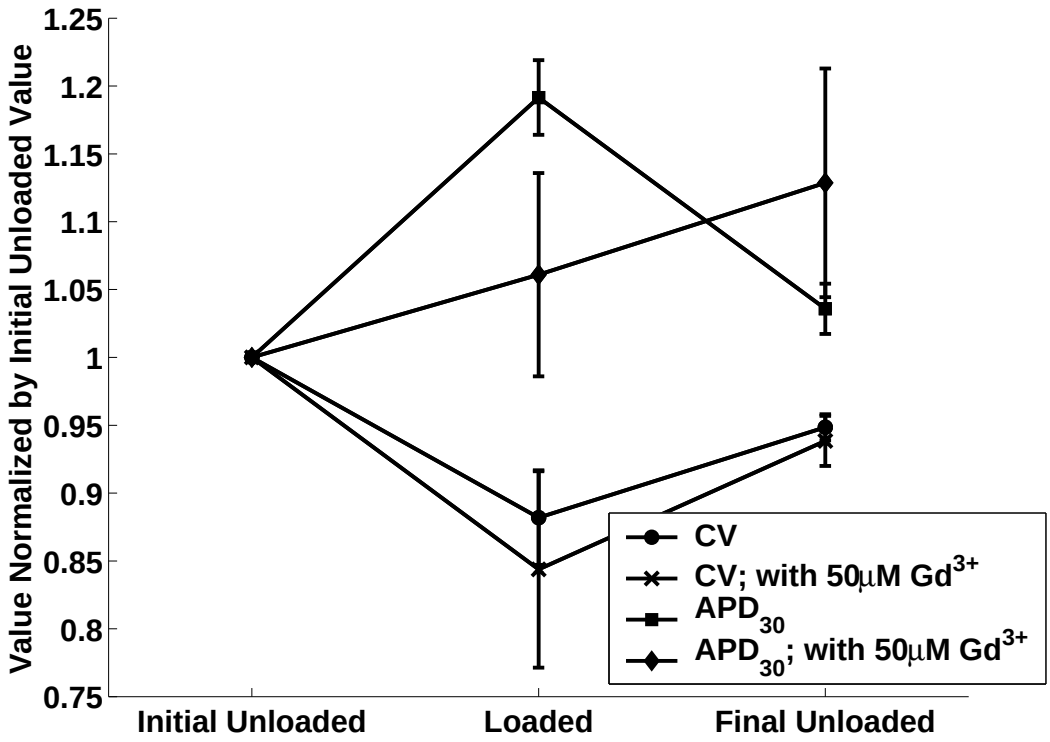

Figure IV.2: Mean ± SEM conduction velocity and action potential duration at 30% repolarization without and with 50 μM gadolinium^{3+}. All values are normalized by the initial unloaded value.

after volume loading. Mean initial unloaded CV was 28.4 ± 2.4 cm/s, decreased 11 ± 3% percent when normokalemic, and decreased at all potassium concentrations, with an overall average decrease of 9 ± 6% ($p = .03$). When load was removed, CV recovered to 94 ± 2% of the initial value when normokalemic, but the overall average CV remained at 91 ± 5% of the initial value. This interaction between recovery of CV from load and perfusate potassium concentration was significant ($p < .01$).

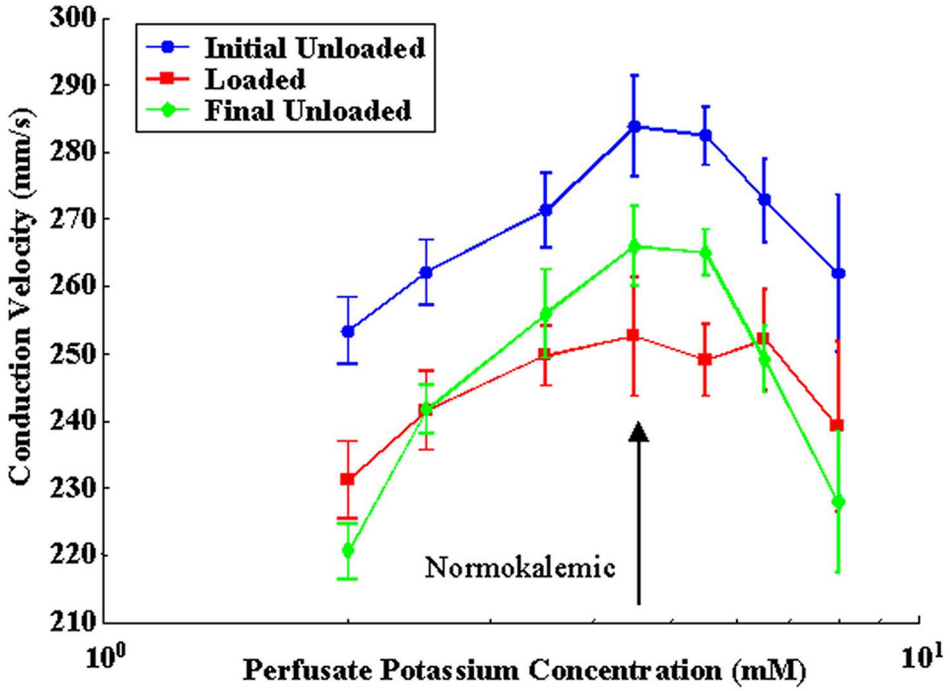

Figure IV.3: The effect of volume loading on conduction velocity at varied perfusate potassium concentrations. (Mean ± SEM)

IV.D.3 Effective Space and Time Constants

Volume loading concurrently slowed conduction and increased the effective cross-fiber space and time constants. Figure IV.4 shows the mean effect of volume loading on effective cross-fiber space and time constants in all 4 hearts. Mean initial unloaded CV was 34.7 ± 2.5 cm/s, decreased 13 ± 1% ($p = .01$) during volume loading, and recovered to 97 ± 3% of initial value when load was removed. However, mean initial unloaded space constant was 0.71 ± 0.06 mm, increased during loading 36 ± 8% ($p = .02$) and recovered to 110 ± 4% of initial value. Similarly, mean initial unloaded time constant was 8.3 ± 2.1ms, increased during loading 64 ± 14% ($p = .02$) and recovered to 140 ± 15% of initial value.

All three relationships were correlated. The correlation coefficient between space constant and time constant was .489, and was statistically significant ($p = .01$). The correlation coefficient between space constant and CV was -.536, and was statistically significant ($p < .01$). The correlation coefficient between time constant and CV was -.726, and was statistically significant ($p < .0001$).

IV.D.4 Carbenoxolone

Inclusion of 50 μM carbenoxolone in the perfusate slowed conduction, decreased effective cross-fiber space constant, and had little consequence on effective cross-fiber time constant; further, it had little consequence on the effect of volume loading on CV, space constant, or time constant. Carbenoxolone caused a 25 ± 5% decrease in unloaded CV ($p = .06$), a 35 ± 7% decrease in space constant ($p = .06$), and a 6 ± 15% decrease in time constant (power was .10 to detect a 10% difference). However, from these new baseline unloaded values, volume loading still decreased CV a further 16 ± 5% ($p = .08$), which recovered to 96 ± 3% of this new baseline value. Volume loading still increased space constant by 48 ± 20% ($p = .25$), which recovered to below the new baseline value to 92 ± 10%, and increased time constant by 67 ± 31% ($p = .17$), which recovered to 140 ± 15% of the new baseline value.

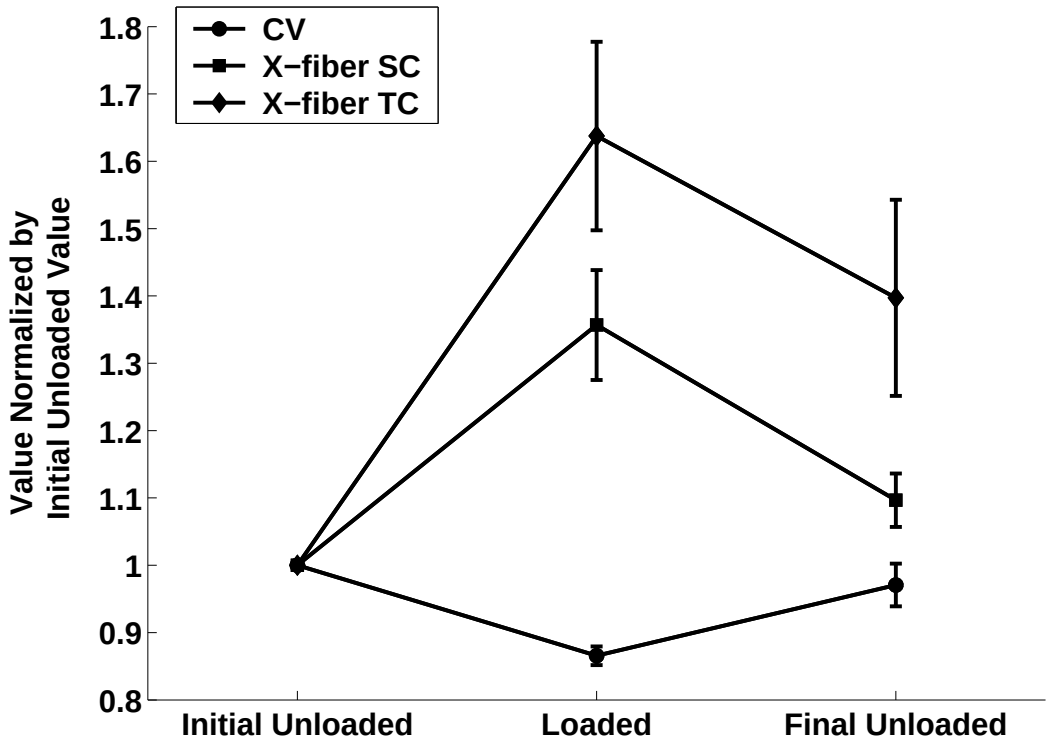

Figure IV.4: Mean ± SEM conduction velocity, effective cross-fiber space constant, and effective cross-fiber time constant as affected by ventricular volume load. All values are normalized by the initial unloaded value.

IV.D.5 Multicellular Fiber Model Conduction Analysis

Inclusion of nominal changes in both intercellular resistance and effective membrane capacitance as implied by the measured changes in effective cross-fiber space and time constants slowed conduction on the same order as that measured. From an initial conduction velocity of 35 cm/s, decreasing only intercellular resistance 45% caused conduction velocity to increase 18%, while increasing only membrane capacitance 64% caused conduction velocity to decrease 23%. A concurrent decrease in resistance and increase in capacitance resulted in a conduction velocity decrease of 10%.

IV.E Discussion

IV.E.1 Stretch-Activated Channels

Previously we have shown that inclusion of the non-specific SAC blocker streptomycin in the perfusate did not significantly alter the effect of volume loading on CV, [3] however, streptomycin had a similar lack of effect for APD. Changes in APD during stretch have been attributed to the action of stretch-activated channels. [25] In this study we observed that loading lengthens APD_{30} and APD_{60}, similar to our previous results, but we further observed that the presence of the SAC blocker Gd^{3+} had an interaction with the effect of volume loading on APD_{30} and APD_{60}, acting as a positive control of the impact of Gd^{3+}. Concurrently, Gd^{3+} had no interaction with the effect of volume loading on CV.

IV.E.2 Membrane Excitability

Varying perfusate potassium concentration had the same previously reported effects on CV. [7] Membrane excitability was significantly altered, as indicated by the large changes in CV. If load caused conduction slowing primarily by altering membrane excitability, then the loaded state would be similar to movement along the unloaded CV vs. perfusate potassium concentration curve, i.e., the loaded curve would be similar to a left- or rightward shift of the unloaded curve. However, volume loading caused conduction slowing at all potassium concentrations, i.e. the loaded curve is similar to a downward shift of the unloaded curve, indicating that load slows conduction independent of altered excitability within the range studied. Moreover, one model study indicates that the slight depolarization from resting potential typically observed during stretch [8] (and attributed to SAC's) would tend to enhance excitability, [26] rather than depress it. Although manipulating excitability did not significantly alter the effect of volume loading on conduction speed near normokalemic concentrations, more extreme depression of excitability did seem to inhibit CV recovery when load was removed.

IV.E.3 Effective Space and Time Constants

Conduction slowing due to volume loading was associated with increases in the effective space and time constants. Our measured effective space constant is on order with that previously reported for the cross-fiber direction using similar methods ($\lambda_T \sim 0.73$ mm). [16] Our measured effective time constant was larger but similar to those membrane time constants previously reported ($\tau_m \sim 2$ - 6 ms). [27, 28] This discrepancy may lie in that these groups used cable-like preparations of myocardial tissue so that cable theory could be used to predict specific myocardial electrical constants, whereas we measured the effective time constant of bulk intact ventricular tissue to get an index of relative capacitive load in different mechanical load states. We did not observe the classic dogbone shape, however, we were looking at the tissue response to the stimulus in the steady-state, some 200 ms after stimulus onset. Others have reported that low stimulus strengths induce an initial dogbone that spreads out non-uniformly, such that the dogbone shape can no longer be easily detected after 10ms. [29]

In one dimension, the effective space constant is proportional to membrane resistance (R_m), and inversely proportional to extracellular and intracellular resistances (R_e, R_i), and the membrane surface to tissue volume ratio (β), while the effective time constant is proportional to membrane resistance and capacitance (C_m). [30]

$$\lambda_T = \sqrt{\frac{R_m}{(R_{iT} + R_{eT})\,\beta}} \qquad \text{and} \qquad \tau = C_m R_m$$

The increase in both space and time constants could be a result of increased membrane resistance, which varies during repolarization and is a function of the current state of the membrane. The Saucerman et al. [22] implementation of the rabbit ventricular myocyte ionic model was used to estimate dynamic membrane resistance

during application of the test stimulus. R_m was estimated as the inverse of the summation of the individual ion dynamic membrane conductances ($1/\Sigma G_i$), where the $G_i = dI_i(t)/dV_m(t)$, where $I_i(t)$ and $V_m(t)$ are the individual ion membrane currents and transmembrane potential, respectively. [31] These derivatives were estimated by calculating the ion membrane currents at perturbations of $V_m(t)$ as in Sampson and Henriquez. [32] This was repeated after including a linear stretch-activated current, as previously suggested, [33] : $I_{SAC} = G_{SAC}(V_m(t) - V_r)$ with $V_r = 10$ mV so that early repolarization was prolonged, as observed in the isolated rabbit heart studies, and G_{SAC} chosen to cause a 10% action potential amplitude depolarization in resting membrane potential. [25] The stimulus was applied at a time such that the stimulus began at approximately 50% repolarization in the original model, similar to experimental studies, and at the same absolute time in the model with the stretch-activated current, consequently, the stimulus began when the membrane was less repolarized compared to the original model. The stimulus amplitude was chosen to cause the same deviation in transmembrane voltage as observed in the experimental studies ($\sim$15% action potential amplitude). These model studies indicate that activation of such a stretch-activated current causes the dynamic membrane resistance to decrease about 2% during the period in which the space constant was measured, and increases about 15% during the period in which the time constant was measured. This indicates that a significant majority of the increases in effective space and time constants is not attributable to increased membrane resistance.

Recently, it has been observed that shear stress of osteocytes induces opening of Cx43 hemi-channels, the predominant connexin type expressed in ventricular myocytes, within 10 minutes from onset of shearing. [34] The increase in effective space constant we measured is indicative of a decrease in longitudinal resistances, and may specifically indicate that ventricular wall stretch caused increased intercellular coupling, possibly by a similar pathway. This may further explain our previous results wherein we saw an unexpected decrease in dispersion

of repolarization during volume loading. [3] An increase in intercellular coupling would be expected to lead to faster conduction. However, computer simulations of propagation in a chain of Luo-Rudy cells indicate that CV in not very sensitive to changes in intercellular resistance at normal levels of cellular coupling. This model study showed that a decrease in CV of 7% required an increase in intercellular resistance of 43%, as most of the resistance to propagation in the fiber direction is composed of myoplasmic resistance. [10] A related experimental study was unable to resolve a difference in CV between synthetic strands of wild-type neonatal cardiomyocytes and strands composed of cells from mice with a 43% reduction in Cx43 expression. Because extracellular resistance in the cross-fiber direction is roughly 0.25 times that of the intracellular resistance, [18] any effect of volume loading on extracellular resistance is expected to have a proportionally less significant effect on conduction velocity.

The increase in measured effective time constant is indicative of an increase in effective membrane capacitance, which is consistent with previous measurements of the effects of stretch on cell membrane. Kohl et al. [35] showed that passive ventricular volume loading to 30 mmHg causes unfolding of slack membrane and integration of caveolae into the sarcolemma. This could lead to an increase in the effective cell membrane surface area to volume ratio, increasing effective membrane capacitance, resulting in increased capacitive electrical load (current sink) on the depolarization wavefront, slowing conduction. Sokabe et al. [36] observed in chick skeletal muscle that a membrane patch placed under tension by suction in the patch pipette resulted in an increase in apparent membrane strain and a proportional increase in patch capacitance, and this has been recently confirmed in rat astrocytes. [37]

IV.E.4 Carbenoxolone

Inclusion of the gap junction uncoupler, carbenoxolone, in the perfusate caused a reduction in both effective space constant and CV, further validating the

methods used to measure the effective space constant. Carbenoxolone was used to test the hypothesis that the increase in effective space constant caused an increase in the effective electrical load on the depolarization wavefront, potentially slowing conduction. However, this implies a biphasic relationship between coupling and CV, and would require that in a moderately uncoupled system, volume loading would increase CV. The carbenoxolone study disproves this hypothesis. Cumulative damage at the stimulus test site and the extended protocol times may explain why the carbenoxolone results have much greater variance, resulting in non statistically-signficant results.

IV.E.5 Multicellular Fiber Model Conduction Analysis

The fiber model results indicate that volume loading may increase effective intercellular coupling, which would result in only slightly faster conduction, as conduction speed in not very sensitive to perturbations in intercellular coupling at normal levels. [10] However, volume loading simultaneously increases the effective membrane capacitance, significantly slowing conduction, as conduction speed is most sensitive to perturbations of membrane capacitance, [38] masking the effect of the increased effective intercellular coupling. The relative contributions of these two competing effects may explain some of the discrepant reports of faster conduction during stretch in several different isolated myocardial tissue preparations, [39, 40, 41, 42] though the discrepancy may also lie in the definition of conduction velocity used, [43] as several reports in whole chamber preparations have observed slowed conduction during stretch. [44, 45, 46, 47] The combination of the two effects in the fiber model resulted in a 10% decrease in conduction speed, while the measured mean decrease in conduction velocity during loading was 13% in the studies in which the effective space and time constants were measured. However, this model study assumed that the entire measured change in effective space and time constants were entirely attributable to a change in effective intercellular resistance and effective membrane capacitance.

IV.F Conclusions

We have shown that slowing of apparent epicardial conduction during myocardial stretch by ventricular volume loading is not significantly attributable to stretch-activated channels or depressed membrane excitability. We have further shown that volume loading is associated with an increase in the effective space and time constants, indicating reduced intercellular resistance and increased effective membrane capacitance, resulting in a net slowing of conduction due to the greater sensitivity of conduction velocity to a change in capacitance. Our model study indicates that increasing effective membrane capacitance and reducing intercellular resistance by amounts suggested by the measured changes in effective space and time constants may be sufficient to account for the degree of conduction slowing observed. Such a mechanism could contribute to re-entrant arrhythmias associated with altered loading conditions.

The text and figures of this chapter, in full, will be submitted for publication. The dissertation author was the primary researcher and author of the work presented here, and any co-authors of this publication directed and supervised the research that forms the basis for this chapter.

Appendix: Relevant MATLAB Code Table of Contents

```
% Additional M-files used in the Analysis of Slowed Conduction During
% Ventricular Volume Loading:
%
% M-files used in:
%    Mills et al.; Mechanisms of Conduction Slowing During Ventricular
%    Volume Loading. (in preparation)
%
%    Contact: Andrew McCulloch, Ph.D.
%             Cardiac Mechanics Research Group
%             Dept. of Bioengineering
%             University of California San Diego
%             9500 Gilman Dr., La Jolla, CA 92093-0412
%             amcculloch@ucsd.edu
%
% Copyright (c) 2005 CMRG - UCSD Bioengineering
%    Any copy of these m-files must include this contents file
%    with this header unaltered.
%
%
%-------------------------------------------------------------------------
%
% Conduction Velocity Analysis and Associated Batch Scripts
%   contvelocmap    - Calculates conduction velocity from activation
%                     times
%   gd3extract      - Setup is useful for comparing a single intervention
%                     on the effect of loading on conduction
%   potassextract   - Setup is useful for comparing a graded-intervention
%                     on the effect of loading on conduction
%
%   Specific Utility Functions:
%       runpotassextract - The working part of 'potassextract'
%
%-------------------------------------------------------------------------
%
% Resistance\Capacitance Analysis
%   capacianalyze       - The engine
%   decayexpfitfunc2D   - Fits data to 2D exponential-type distribution
%
%   Specific Utility Functions:
%       addARBWpoint    - Assitant in creating ARBW
%       Bobgline        - Selection of line along which a space constant
%                         is estimated and selects region to include in
%                         2D fit
%       capacianalyzemidpthelper    - midtpt helper
%       decayexpfitfunc     - should be rolled into 'expfitfunc', used by
%                             'Bobgline'
%       decayexpfitfunc2Doptiminteract  - go-between function
%       fsdtofsifffunc      - Assistant in adjusting the difference
%                             between Fsi and Fsd
%       gendecayexp         - should be rolled into 'genincexp'
```

```
% getM1M2relationship - Assistant for fitting to
%                        'rothshapefunc_m1m2linked'
% rothshapefunc3      - Fit theory to data
% rothshapefunc3_m1m2linked   - Fit theory to data, with
%                               M1-M2 restriction
% normrange           - Assitant in setting the range for the
%                       normalization AP
% plotsforcapacianalyze       - Plots relevant data
% resistranges        - Assistant in setting the steady-state
%                       range for measuring the space constant
% runcapacianalyze    - The working part of 'capacianalyze'
% selectrmscutofffunc - Assistant in selecting the RMS cutoff
%
%-------------------------------------------------------------------------
%
% Modeling of Conduction Along a Fiber
%   multicalc                   - Setup for running repeated model runs
%                                 using varied parameters
%   Bobfiberdiscretemulticalc   - Initializes the fiber model
%
%
%   Specific Utility Functions:
%       solvediscretefiber  - Solves a specific fiber problem
%       JSrabBob            - Jeff Saucerman's implementation of a rabbit
%                             ventricular myocyte model
```

References

[1] Stevenson WG, Stevenson LW. Prevention of sudden death in heart failure. *J Cardiovasc Electrophysiol.* 2001;12(1):112-114.

[2] Kuo CS, et al. Characteristics and possible mechanism of ventricular arrhythmia dependent on the dispersion of action potential durations. *Circulation.* 1983;67(6):1356-1367.

[3] Sung D, et al. Ventricular filling slows epicardial conduction and increases action potential duration in an optical mapping study of the isolated rabbit heart. *J Cardiovasc Electrophysiol.* 2003;14(7):739-749.

[4] Hu H, Sachs F. Stretch-activated ion channels in the heart. *J Mol Cell Cardiol.* 1997;29(6):1511-1523.

[5] Roden DM, et al. Cardiac ion channels. *Annu Rev Physiol.* 2002;64431-475.

[6] Nygren A, Giles WR. Mathematical simulation of slowing of cardiac conduction velocity by elevated extracellular [k+] in a human atrial strand. *Ann Biomed Eng.* 2000;28(8):951-957.

[7] Rohr S, Kucera JP, Kleber AG. Slow conduction in cardiac tissue, i: Effects of a reduction of excitability versus a reduction of electrical coupling on microconduction. *Circ Res.* 1998;83(8):781-794.

[8] Franz MR. Mechano-electrical feedback in ventricular myocardium. *Cardiovasc Res.* 1996;32(1):15-24.

[9] Kootsey JM. Electrical propagation in distributed cardiac tissue. In: Glass L, Hunter P, McCulloch AD, eds. *Theory of heart: Biomechanics, biophysics, and nonlinear dynamics of cardiac function.* New York: Springer-Verlag; 1991:391-403.

[10] Thomas SP, et al. Impulse propagation in synthetic strands of neonatal cardiac myocytes with genetically reduced levels of connexin43. *Circ Res.* 2003;92(11):1209-1216.

[11] Gutstein DE, et al. The organization of adherens junctions and desmosomes at the cardiac intercalated disc is independent of gap junctions. *J Cell Sci.* 2003;116(Pt 5):875-885.

[12] Shaw RM, Rudy Y. Ionic mechanisms of propagation in cardiac tissue. Roles of the sodium and l-type calcium currents during reduced excitability and decreased gap junction coupling. *Circulation Research.* 1997;81(5):727-741.

[13] Sung D, Omens JH, McCulloch AD. Model-based analysis of optically mapped epicardial activation patterns and conduction velocity. *Ann Biomed Eng.* 2000;28(9):1085-1092.

[14] Sung D, et al. Phase shifting prior to spatial filtering enhances optical recordings of cardiac action potential propagation. *Ann Biomed Eng.* 2001;29(10):854-861.

[15] Bayly PV, et al. Estimation of conduction velocity vector fields from epicardial mapping data. *IEEE Trans Biomed Eng.* 1998;45(5):563-571.

[16] Poelzing S, Roth BJ, Rosenbaum DS. Optical measurements reveal nature of intercellular coupling across ventricular wall. *Am J Physiol Heart Circ Physiol.* 2005;289(4):H1428-1435.

[17] Roth BJ. Approximate analytical solutions to the bidomain equations with unequal anisotropy ratios. *Phys Rev E Stat Nonlin Soft Matter Phys.* 1997;55(2):1819-1826.

[18] Roth BJ. Electrical conductivity values used with the bidomain model of cardiac tissue. *IEEE Trans Biomed Eng.* 1997;44(4):326-328.

[19] de Groot JR, et al. Conduction slowing by the gap junctional uncoupler carbenoxolone. *Cardiovasc Res.* 2003;60(2):288-297.

[20] Cohen J. *Statistical power analysis for the behavioral sciences.* New York: Academic Press; 1977.

[21] Shaw RM, Rudy Y. Electrophysiologic effects of acute myocardial ischemia. A mechanistic investigation of action potential conduction and conduction failure. *Circ Res.* 1997;80(1):124-138.

[22] Saucerman JJ, et al. Modeling beta-adrenergic control of cardiac myocyte contractility in silico. *J Biol Chem.* 2003;278(48):47997-48003.

[23] Puglisi JL, Bers DM. Labheart: An interactive computer model of rabbit ventricular myocyte ion channels and ca transport. *Am J Physiol Cell Physiol.* 2001;281(6):C2049-2060.

[24] Luo CH, Rudy Y. A dynamic model of the cardiac ventricular action potential. I. Simulations of ionic currents and concentration changes. *Circ Res.* 1994;74(6):1071-1096.

[25] Zabel M, et al. Stretch-induced voltage changes in the isolated beating heart: Importance of the timing of stretch and implications for stretch-activated ion channels. *Cardiovascular Research.* 1996;32(1):120-130.

[26] Riemer TL, Sobie EA, Tung L. Stretch-induced changes in arrhythmogenesis and excitability in experimentally based heart cell models. *American Journal of Physiology.* 1998;275(2 Pt 2):H431-442.

[27] Daut J. The passive electrical properties of guinea-pig ventricular muscle as examined with a voltage-clamp technique. *J Physiol.* 1982;330221-242.

[28] Kleber AG, Riegger CB. Electrical constants of arterially perfused rabbit papillary muscle. *J Physiol*. 1987;385307-324.

[29] Sambelashvili AT, Nikolski VP, Efimov IR. Nonlinear effects in subthreshold virtual electrode polarization. *Am J Physiol Heart Circ Physiol*. 2003;284(6):H2368-2374.

[30] Jack J, Noble D, Tsien R. *Electric current flow in excitable cells*. Oxford: Clarendon Press; 1975.

[31] Wu J, Zipes DP. Effects of spatial segmentation in the continuous model of excitation propagation in cardiac muscle. *J Cardiovasc Electrophysiol*. 1999;10(7):965-972.

[32] Sampson KJ, Henriquez CS. Electrotonic influences on action potential duration dispersion in small hearts: A simulation study. *Am J Physiol Heart Circ Physiol*. 2005;289(1):H350-360.

[33] Zeng T, Bett GC, Sachs F. Stretch-activated whole cell currents in adult rat cardiac myocytes. *Am J Physiol Heart Circ Physiol*. 2000;278(2):H548-557.

[34] Cherian PP, et al. Mechanical strain opens connexin 43 hemichannels in osteocytes: A novel mechanism for the release of prostaglandin. *Mol Biol Cell*. 2005.

[35] Kohl P, Cooper PJ, Holloway H. Effects of acute ventricular volume manipulation on in situ cardiomyocyte cell membrane configuration. *Prog Biophys Mol Biol*. 2003;82(1-3):221-227.

[36] Sokabe M, Sachs F, Jing ZQ. Quantitative video microscopy of patch clamped membranes stress, strain, capacitance, and stretch channel activation. *Biophys J*. 1991;59(3):722-728.

[37] Suchyna TM, Besch SR, Sachs F. Dynamic regulation of mechanosensitive channels: Capacitance used to monitor patch tension in real time. *Physical Biology*. 2004;1(1):1-18.

[38] Lieberman M, et al. Low conduction in cardiac muscle. Biophysical model. *Biophys J*. 1973;13(1):37-55.

[39] Penefsky ZJ, Hoffman BF. Effects of stretch on mechanical and electrical properties of cardiac muscle. *Am J Physiol*. 1963;204(3):433-438.

[40] Deck KA. [changes in the resting potential and the cable properties of purkinje fibers during stretch]. *Pflugers Arch Gesamte Physiol Menschen Tiere*. 1964;280131-140.

[41] Dominguez G, Fozzard HA. Effect of stretch on conduction velocity and cable properties of cardiac purkinje fibers. *Am J Physiol*. 1979;237(3):C119-124.

[42] Rosen MR, Legato MJ, Weiss RM. Developmental changes in impulse conduction in the canine heart. *Am J Physiol*. 1981;240(4):H546-554.

[43] Mills RW, Narayan SM, McCulloch AD. The effects of wall stretch on ventricular conduction and refractoriness in the whole heart. In: Kohl P, Sachs F, Franz MR, eds. *Cardiac mechano-electric feedback and arrhythmias: From pipette to patient*. Philadelphia: Saunders/Elsevier; 2005:Chapter 14.

[44] Sideris DA, et al. Effect of acute ventricular pressure changes on qrs duration. *J Electrocardiol*. 1994;27(3):199-202.

[45] Zabel M, Portnoy S, Franz MR. Effect of sustained load on dispersion of ventricular repolarization and conduction time in the isolated intact rabbit heart. *J Cardiovasc Electrophysiol*. 1996;7(1):9-16.

[46] Chorro FJ, et al. [acute changes in wavelength of the process of auricular activation induced by stretching. Experimental study]. *Rev Esp Cardiol*. 1998;51(11):874-883.

[47] Eijsbouts SC, et al. Effects of acute atrial dilation on heterogeneity in conduction in the isolated rabbit heart. *J Cardiovasc Electrophysiol*. 2003;14(3):269-278.

Chapter V

Conclusions

Several studies have linked increased myocardial strain (wall stretch) with atrial and ventricular arrhythmias. [1] Although the precise mechanisms for these loading related rhythm disturbances remain unclear, the predominant mechanism underlying ventricular arrhythmias associated with mechanical dysfunction is reentrant conduction, [2] which is promoted and sustained by slowed conduction. Passive ventricular volume loading in the Langendorff-perfused isolated rabbit heart has been shown to slow conduction. [3]

The objective of this dissertation was to investigate the potential mechanisms of conduction slowing during ventricular volume loading in the isolated heart. Though the focus of this work was to investigate a physiologically-based conduction response to a mechanical stimulus, this work required validation of previous observations of conduction slowing using optical mapping, and the extensive development of data handling algorithms, which continue to be useful in other studies using optical mapping of Langendorff-perfused hearts.

We chose the non-contact optical mapping technique to record epicardial electrical activity, as this technique does not introduce mechanical artifact, which may be present in other methods of measuring electrical activity, such as monophasic action potential electrode and microelectrodes, because these methods require contact with the myocardium. [4] This technique is also advantageous

in that it is capable of high-resolution multi-site mapping of electrical activity, including an accurate representation of local repolarization. [5, 6] Charge-coupled-device cameras were chosen to acquire this mapping, as they currently have a superior combination of spatial resolution and dynamic range compared to other devices, but at the cost of lower signal-to-noise ratios. As part of this work, we validated the utility of a computationally expensive phase-shift filtering technique that enhances signal-to-noise without distorting the optical action potential upstroke. Further improvements were made to the filtering and analysis algorithms to improve efficiency and accuracy.

Previous experimental observations of conduction slowing during passive ventricular volume loading were validated by eliminating several potential non-physiological mechanisms. We found that conduction slowing is not a consequence of global or regional ischemia, or a decrease in epicardial surface temperature, all of which could be caused by increased resistance to perfusion during intraventricular balloon inflation. We also found that conduction slowing during volume loading still occurs in the absence of the agents di-4-ANEPPS and 2,3-butanedione monoxime, which were necessary for the optical mapping technique. Further, these studies show that conduction slowing and action potential lengthening are correlated with the degree of loading within a physiological range, as incremental increases in load incrementally affect conduction and action potential duration. These studies also led to an improved isolated heart preparation, wherein epicardial surface temperature is less impacted by loading.

Several potential physiological mechanisms of conduction slowing during ventricular volume loading were investigated. We found that stretch-activated channels do not significantly contribute, which is consistent with our previous findings using a different stretch-activated channel blocker, streptomycin. [3] However, in this study we had a positive control of the activity of gadolinium^{3+} blocking stretch-activated channels. We also found that volume loading does not significantly depress membrane excitability, which is consistent with a model study of

the effect of stretch on membrane excitability. [7] Finally, we found that ventricular loading caused an increase in effective space and time constants, suggesting that loading may reduce intercellular resistance and increase effective membrane capacitance, resulting in a net slowing of conduction due to the greater sensitivity of conduction velocity to a change in capacitance. These conclusions are consistent with findings that shear stress can induce opening of Cx43 (the predominant connexin type expressed in ventricular myocytes gap junctions) hemi-channels in osteocytes, [8], that membrane strain increases membrane capacitance, [9] and that ventricular volume loading can increase whole-cell capacitance by causing the incorporation of sequestered membrane into the sarcolemma. Our model study indicates that increasing effective membrane capacitance and reducing intercellular resistance by magnitudes suggested by the measured changes in effective space and time constants may be sufficient to account for the degree of conduction slowing observed.

V.A Limitations and Future Work

The pharmacological agent, 2,3-butanedione monoxime (BDM) was used to eliminate motion artifact in the optically acquired recordings of myocardial electrical activity. BDM causes a shift towards more weakly bound actin-myosin complexes, reducing fiber tension by increasing phosphate binding and by direct action on the crossbridges. [10] In addition BDM promotes Ca^{2+} release from the sarcoplasmic reticulum, [11] suppresses the L-type Ca^{2+} channel and the transient outward current, [12] the Na^{+}/Ca^{2+} exchanger, [13] and causes some uncoupling of gap junctions. [14] Despite all of these effects, we observed that volume loading slows conduction even when BDM is not present. [3] However, further studies without the use of this agent would improve the veracity of our findings. Further improvements to the optical mapping technique currently in progress will obviate

the use of BDM through a combination of fluorescence ratiometry and optical flow techniques to remove motion artifact.

Other studies that have used optical mapping to observe myocardial electrical response to current injection, and thus measure the effective space constant of the tissue, have used sub-threshold stimuli applied to resting membrane. [15, 16] However, these studies were performed using a lower spatial resolution (16×16) photo-diode array (PDA), which tend to have superior signal-to-noise ratios than the charge-coupled-device (CCD) camera used in our studies. We used a CCD camera due to its superior spatial resolution (128×126), but sub-threshold stimuli could not be resolved from the noise in preliminary studies. Consequently, we used supra-threshold stimuli applied during repolarization, during which the effective membrane resistance is not constant. The effective space constant is dependent on membrane resistance, however, measurements of effective space constant were made after the transmembrane voltage achieved steady-state (post-repolarization). The effective time constant is also dependent on effective membrane resistance, however, a few stimuli that did not elicit break excitation were used to measure the effective time constant at the stimulus break (post-repolarization), and corroborated the increase in time constant during loading. Repeated studies using a PDA and sub-threshold stimuli could confirm our findings.

The conclusions of increased coupling and capacitance are based on theory applied to the measurements of effective space and time constants, which are also dependent on membrane resistance and extracellular resistance (space constant only). However, independent studies of stretch of cellular preparations are consistent with these conclusions. [8, 9] Further cellular studies would be useful in confirming these conclusions and elucidating specific mechanisms behind increases in intercellular coupling and capacitance during stretch, by attempting to block these increases. Gap junctions are regulated by local ion concentrations and several pathways that are influenced by stretch, [17] and tend to co-localize with several cellular structural elements, [18] giving several suitable targets for at-

tempted disruption of an increase in intercellular coupling during stretch. Cellular studies in which whole-cell capacitance of myocytes is monitored during stretch could confirm an increase. Unfortunately, previous studies in myocytes have only measured stretch of membrane patches. [9, 19] Capacitance could also be increased by integration of caveolae and sheltered membrane folds into actively capacitive membrane during ventricular volume loading. [20] Studies of stretch on whole-cell capacitance in preparations from caveolin deficient mice [21] could elucidate the relative contribution of this mechanism, while studies in preparations that have been treated with the actin filament disrupter, cytochalasin D, may be sufficient to disrupt membrane unfolding.

Finally, it would be beneficial to have a more temporally refined assessment of the time course of the slowing of conduction and changes in effective space and time constants after the onset of volume loading, since our measurements were taken 1 minute after loading. An immediate slowing of conduction would indicate a direct mechanical effect on biophysical properties, while conduction slowing that develops over a period of a couple of minutes could be the result of cellular signaling.

V.B Implications

These studies suggest that reentrant ventricular arrhythmias associated with increased myocardial strain and mechanical dysfunction may be promoted and sustained by an increased effective membrane capacitance. Consequently, decreasing membrane capacitance by treatment with growth hormone [22] or penetratin [23] may be cardioprotective against these arrhythmias.

References

[1] Stevenson WG, Stevenson LW. Prevention of sudden death in heart failure. *J Cardiovasc Electrophysiol.* 2001;12(1):112-114.

[2] Kuo CS, et al. Characteristics and possible mechanism of ventricular arrhythmia dependent on the dispersion of action potential durations. *Circulation.* 1983;67(6):1356-1367.

[3] Sung D, et al. Ventricular filling slows epicardial conduction and increases action potential duration in an optical mapping study of the isolated rabbit heart. *J Cardiovasc Electrophysiol.* 2003;14(7):739-749.

[4] Tranquillo JV, et al. Genesis of the monophasic action potential: Role of interstitial resistance and boundary gradients. *Am J Physiol Heart Circ Physiol.* 2004;286(4):H1370-1381.

[5] Efimov IR, Nikolski VP, Salama G. Optical imaging of the heart. *Circ Res.* 2004;95(1):21-33.

[6] Knisley SB, et al. Ratiometry of transmembrane voltage-sensitive fluorescent dye emission in hearts. *Am J Physiol Heart Circ Physiol.* 2000;279(3):H1421-1433.

[7] Riemer TL, Sobie EA, Tung L. Stretch-induced changes in arrhythmogenesis and excitability in experimentally based heart cell models. *American Journal of Physiology.* 1998;275(2 Pt 2):H431-442.

[8] Cherian PP, et al. Mechanical strain opens connexin 43 hemichannels in osteocytes: A novel mechanism for the release of prostaglandin. *Mol Biol Cell.* 2005.

[9] Sokabe M, Sachs F, Jing ZQ. Quantitative video microscopy of patch clamped membranes stress, strain, capacitance, and stretch channel activation. *Biophys J.* 1991;59(3):722-728.

[10] McKillop DF, et al. The influence of 2,3-butanedione 2-monoxime (bdm) on the interaction between actin and myosin in solution and in skinned muscle fibres. *J Muscle Res Cell Motil.* 1994;15(3):309-318.

[11] Adams W, Trafford AW, Eisner DA. 2,3-butanedione monoxime (bdm) decreases sarcoplasmic reticulum ca content by stimulating ca release in isolated rat ventricular myocytes. *Pflugers Arch.* 1998;436(5):776-781.

[12] Coulombe A, et al. Effect of 2,3-butanedione 2-monoxime on slow inward and transient outward currents in rat ventricular myocytes. *J Mol Cell Cardiol.* 1990;22(8):921-932.

[13] Watanabe Y, et al. Inhibitory effect of 2,3-butanedione monoxime (bdm) on na(+)/ca(2+) exchange current in guinea-pig cardiac ventricular myocytes. *Br J Pharmacol*. 2001;132(6):1317-1325.

[14] Verrecchia F, Hervé JC. Reversible blockade of gap junctional communication by 2,3-butanedione monoxime in rat cardiac myocytes. *American Journal of Physiology*. 1997;272(3 Pt 1):C875-885.

[15] Akar FG, Roth BJ, Rosenbaum DS. Optical measurement of cell-to-cell coupling in intact heart using subthreshold electrical stimulation. *Am J Physiol Heart Circ Physiol*. 2001;281(2):H533-542.

[16] Poelzing S, Roth BJ, Rosenbaum DS. Optical measurements reveal nature of intercellular coupling across ventricular wall. *Am J Physiol Heart Circ Physiol*. 2005;289(4):H1428-1435.

[17] Dhein S. *Cardiac gap junctions*. New York: Karger; 1998.

[18] Gutstein DE, et al. The organization of adherens junctions and desmosomes at the cardiac intercalated disc is independent of gap junctions. *J Cell Sci*. 2003;116(Pt 5):875-885.

[19] Suchyna TM, Besch SR, Sachs F. Dynamic regulation of mechanosensitive channels: Capacitance used to monitor patch tension in real time. *Physical Biology*. 2004;1(1):1-18.

[20] Kohl P, Cooper PJ, Holloway H. Effects of acute ventricular volume manipulation on in situ cardiomyocyte cell membrane configuration. *Prog Biophys Mol Biol*. 2003;82(1-3):221-227.

[21] Razani B, Lisanti MP. Caveolin-deficient mice: Insights into caveolar function human disease. *J Clin Invest*. 2001;108(11):1553-1561.

[22] De Luca A, et al. Effects of chronic growth hormone treatment in aged rats on the biophysical and pharmacological properties of skeletal muscle chloride channels. *Br J Pharmacol*. 1997;121(3):369-374.

[23] Salamon Z, Lindblom G, Tollin G. Plasmon-waveguide resonance and impedance spectroscopy studies of the interaction between penetratin and supported lipid bilayer membranes. *Biophys J*. 2003;84(3):1796-1807.